

Asynchronous Policy Evaluation in Distributed Reinforcement Learning over Networks

Xingyu Sha[‡] Jiaqi Zhang[‡] Kaiqing Zhang[†] Keyou You[‡] Tamer Başar[†]

November 11, 2021

Abstract

This paper proposes a *fully asynchronous* scheme for policy evaluation of distributed reinforcement learning (DisRL) over peer-to-peer networks. Without any form of coordination, nodes can communicate with neighbors and compute their local variables using (possibly) delayed information at any time, which is in sharp contrast to the asynchronous gossip. Thus, the proposed scheme fully takes advantage of the distributed setting. We prove that our method converges at a linear rate $\mathcal{O}(c^k)$ where $c \in (0, 1)$ and k increases by one no matter on which node updates, showing the computational advantage by reducing the amount of synchronization. Numerical experiments show that our method speeds up linearly w.r.t. the number of nodes, and is robust to straggler nodes. To the best of our knowledge, our work is the first theoretical analysis for asynchronous update in DisRL, including the *parallel RL* domain advocated by A3C.

1 Introduction

Reinforcement learning (RL) aims to guide decision makers (a.k.a. agents) to learn optimal policies/strategies by interacting with the environment, which has achieved super-human performance in many tasks [13, 16]. This work considers the *distributed reinforcement learning (DisRL)* problem over a directed *peer-to-peer (p2p)* network, which includes two distinct RL setups depending on the role of the network node. One is the so-called the multi-agent RL (MARL) in which network nodes are the acting agents of the MARL [20, 41, 48], and has proved its capability in e-sports [40], swarm robotics [21], traffic control [39] and resource allocation [25], etc. The other is the parallel RL where network nodes are designed to jointly solve a large-scale RL problem over decentralized sets of experiences [10, 26].

As the MARL in [8, 20, 30, 48, 49], each agent of the p2p network has access to a local dataset and exchanges information only with a subset of agents to learn globally. For the parallel RL, the approach with a central node to communicate with all the other nodes has been already adopted in the A3C [26], which is well-known as the server/worker configuration. However, it is practically restrained by the vulnerability of the central node [22] and can also be considered as a star p2p network.

In the DisRL, all the nodes over the p2p network participate in the learning process, either synchronously or asynchronously. In a synchronous model, all nodes communicate with neighbors and compute their local variables with a global clock/counter for synchronization [33, 36], which may be hard to implement in large-scale systems [4, 42], and suffer from deadlocks [1, 23]. While synchronous algorithms are easier to design, their efficiency is greatly dragged by the slowest node in heterogenous cases. To facilitate the implementation and improve the computational efficiency, we adopt the *fully asynchronous* model in [11, Section 2] where every node can communicate with its neighbors and update its local variables

[‡]X. Sha, J. Zhang and K. You are with the Department of Automation and BNRist, Tsinghua University, Beijing 100084, China. Emails: shaxy18@mails.tsinghua.edu.cn, zjq16@mails.tsinghua.edu.cn, youky@tsinghua.edu.cn.

[†]K. Zhang and T. Başar are with Department of Electrical and Computer Engineering and Coordinated Science Laboratory, University of Illinois at Urbana-Champaign, Urbana, IL 61801 USA. Emails: kzhang66@illinois.edu, basar1@illinois.edu.

using (possibly) delayed information at any time. Since we aim for *directed* communications, each node does not need any coordination with other nodes. This is in sharp contrast to the random asynchronous gossip where only a pair of nodes concurrently update via pairwise averaging per round [3, 23, 43] and may create deadlocks in practice, as well as vulnerable to information delays. It can also be problematic if a node is unable to respond or has only access to its local dataset. In fact, the advantages of the fully asynchronous model has been well documented in distributed learning and optimization both empirically and theoretically, see e.g. [1, 2, 37, 46]. In this work, we are the first to study the fully asynchronous policy evaluation task in the DisRL over directed p2p networks, which is essential to the actor-critic RL algorithms [14, 34].

The MARL has already demonstrated its powerfulness in several challenging tasks in [12, 40] and [15], although a solid theoretical foundation remains to be established. [48] propose two multi-agent actor-critic methods and show almost sure convergence for linear approximation. As an important problem, the policy evaluation of the MARL has been studied in [5, 7, 8, 31, 41], among which [7, 8, 41] and [5] are closely related to this work as we also use the primal-dual reformulation of the mean square projected Bellman error (MSPBE) objective function and obtain a linear convergence guarantee. Striking differences from this work are that [41] only consider the synchronous case and require each agent to select the same sample per learning iteration. Thus, they are unable to handle the decentralized datasets and the space complexity increases linearly with respect to the data amount. This has been resolved in [5] by designing consensus-based distributed (but synchronous) algorithms over undirected p2p networks. More general works on the MARL setting can be found in [47]. To our knowledge, we are the first to exploit the fully asynchronous model in the MARL.

Importantly, our fully asynchronous algorithm for MARL can also be easily used to accelerate the policy evaluation of the parallel RL over a directed p2p network. The abundant theoretical analysis for the RL can be extended to the parallel RL [6] which has registered great success in complex control tasks [10, 19]. The A3C with the server/worker configuration [26] is the first asynchronous parallel RL, where the asynchronism has stabilizing advantages in the training process. In GALA [3], the authors replace the central node of A3C with a group of learners organized over a p2p network. Thus each learner only coordinates with its subordinate worker to perceive RL experiences. GALA outperforms A3C in both data efficiency and robustness, and the learners of GALA have policies keeping within an ϵ -ball of one-another when being trained in the random asynchronous model. In our work, we can explicitly give the convergence rate of the fully asynchronous model in the worst-case sense for the parallel RL over directed p2p networks.

Interestingly, [2] shows that a naive extension of the synchronous gradient-push optimization algorithm to the fully asynchronous model may even diverge. This issue has been solved by designing a novel adaptive learning rate [46] or leveraging the gradient tracking method [37, 44], which inspires the design of our algorithm. There are also works on asynchronous settings in different contexts. For example, [17, 24] design asynchronous *coordinate descent* algorithms which are not amenable to p2p networks.

In comparison, our main contribution can be summarized as follows: (a) We propose a unified policy evaluation formulation for both the collaborative MARL and parallel RL. (b) We design a fully asynchronous policy evaluation algorithm over a p2p network with *directed* communications, which achieves a linear convergence rate within a certain level of tolerance. (c) We develop a novel augmented graph approach to handle full asynchrony and delays for solving the distributed saddle-point problems of this work. (d) We validate via simulations that our algorithm achieves a linear speedup with respect to the number of computational nodes and is robust to straggler nodes.

Notations of this paper are defined below.

- $[\mathbf{a}_1, \dots, \mathbf{a}_n]$ and $[\mathbf{a}_1; \dots; \mathbf{a}_n]$ denote the horizontal stack and vertical stack of $\mathbf{a}_1, \dots, \mathbf{a}_n$, respectively.
- $\|\cdot\|_2$ denotes the l_2 -norm of a vector or matrix. $\|\cdot\|_F$ denotes the matrix Frobenius norm. $\|\cdot\|_D$ denotes the D -norm, i.e., $\|\mathbf{x}\|_D = (\mathbf{x}^\top D \mathbf{x})^{1/2}$ if the matrix D is semi-positive definite.
- \mathbf{A} is called a row-stochastic matrix if each element of \mathbf{A} is nonnegative and $\mathbf{A}\mathbf{1} = \mathbf{1}$. \mathbf{A} is column-stochastic if \mathbf{A}^\top is row-stochastic.

- $[A]_{ij}$ denotes the element in row i and column j of A .
- $\lambda_{\max}(A)$ and $\lambda_{\min}(A)$ denote the largest and smallest eigenvalues of A , respectively.
- $\mathbf{1}_n$ and $\mathbf{0}_n$ denote the n -dimensional vector with all ones and all zeros, respectively.
- The distance between nodes i and j in a graph \mathcal{G} is the smallest number of edges among all paths from i to j . We use $d_g \leq n$ to denote the diameter of a strongly connected graph \mathcal{G} , which is the largest distance between any pair of nodes.

2 Problem formulation

2.1 The DisRL over networks

Let $\mathcal{G} = (\mathcal{V}, \mathcal{E})$ be a directed p2p network, where $\mathcal{V} = \{1, \dots, n\}$ is the set of network nodes and $\mathcal{E} \subseteq \mathcal{V} \times \mathcal{V}$ is the set of edges. Depending on the specific DisRL setting, a node can be either a learner in the parallel RL, or an acting agent in the MARL. A directed edge $(i, j) \in \mathcal{E}$ means that node i can directly send information to node j . Denote $\mathcal{N}_{in}^i = \{j | (j, i) \in \mathcal{E}\} \cup \{i\}$ and $\mathcal{N}_{out}^i = \{j | (i, j) \in \mathcal{E}\} \cup \{i\}$ as the sets of in-neighbors and out-neighbors of node i , respectively.

The DisRL over a p2p network is based on a discrete Markov decision process (MDP) with a tuple $(\mathcal{S}, \prod_{i=1}^n \mathcal{A}_i, \mathcal{P}, \{\mathcal{R}_i\}_{i=1}^n, \gamma, \mathcal{G})$, where the finite sets \mathcal{S} and \mathcal{A}_i denote the state space and the action space of node i in \mathcal{G} , respectively. $\mathcal{P}(s'|s, \mathbf{a})$ is the probability of transitioning from $s \in \mathcal{S}$ to $s' \in \mathcal{S}$ under an action $\mathbf{a} \in \mathcal{A} := \prod_{i=1}^n \mathcal{A}_i$. $\mathcal{R}_i = \mathcal{R}_i(s, \mathbf{a})$ is the reward perceived by a single node i . $\gamma \in (0, 1)$ is the discount factor. \mathcal{G} is used to model the interactions among nodes.

A stochastic policy $\pi(\mathbf{a}|s)$ is the conditional probability of taking action \mathbf{a} given a specific state s . If we focus on a target policy π , the fixed transition probability matrix is denoted as \mathcal{P}^π , whose (s, s') -th entries are given by $[\mathcal{P}^\pi]_{s, s'} = \mathcal{P}(s'|s, \pi) = \sum_{\mathbf{a} \in \mathcal{A}} \pi(\mathbf{a}|s) \cdot \mathcal{P}(s'|s, \mathbf{a})$. Let $\mathcal{R}^\pi(s) = \frac{1}{n} \sum_{i=1}^n \mathcal{R}_i^\pi(s)$, where $\mathcal{R}_i^\pi(s) = \mathbb{E}_{\mathbf{a} \sim \pi(\cdot|s)}[\mathcal{R}_i(s, \mathbf{a})]$ is denoted as the expected reward at state s if the group follows the policy π .

2.2 Policy evaluation

Under a given policy π , the value function $V^\pi(s)$ is defined as $V^\pi(s) = \mathbb{E}[\sum_{t=0}^{\infty} \gamma^t \mathcal{R}^\pi(s(t)) | s(0) = s, \pi]$ and its vector form is $\mathbf{V}^\pi \in \mathbb{R}^{|\mathcal{S}|}$. Clearly, it satisfies the Bellman function [34], $\mathbf{V}^\pi = \mathcal{R}^\pi + \gamma \mathcal{P}^\pi \mathbf{V}^\pi$, where \mathcal{R}^π is obtained by stacking up $\mathcal{R}^\pi(s)$. In this work, we adopt a linear approximator to evaluate the value function, e.g., $V^\pi(s) \approx \phi^\top(s) \theta$, where $\phi(s) \in \mathbb{R}^d$ is a feature vector corresponding to s .

Our problem aims to finding a $\theta \in \mathbb{R}^d$ such that $\mathbf{V}_\theta = \Phi \theta \approx \mathbf{V}^\pi$ by minimizing the mean squared projected Bellman error (MSPBE) $J(\theta) = \frac{1}{2} \|\Pi_\Phi(\mathbf{V}_\theta - \gamma \mathcal{P}^\pi \mathbf{V}_\theta - \mathcal{R}^\pi)\|_D^2 + \frac{\rho}{2} \|\theta\|^2$, where $D = \text{diag}(\mu^\pi(s))$ and $\mu^\pi(s)$ is the stationary distribution of states under π , Π_Φ is the projection onto subspace $\{\Phi \theta\}$, and $\frac{\rho}{2} \|\theta\|^2$ is the regularization term. By [35], the MSPBE loss function is equivalent to

$$J(\theta) = \frac{1}{2} \|\mathbf{A} \theta - \mathbf{b}\|_{\mathbf{C}^{-1}}^2 + \frac{\rho}{2} \|\theta\|^2 \quad (1)$$

where ϕ_t is the short for $\phi(s(t))$, and $\mathbf{A} = \mathbb{E}_{\mu^\pi}[\phi_t(\phi_t - \gamma \phi_{t+1})^\top]$, $\mathbf{b} = \mathbb{E}_{\mu^\pi}[\mathcal{R}^\pi(s(t)) \phi_t]$, $\mathbf{C} = \mathbb{E}_{\mu^\pi}[\phi_t \phi_t^\top]$. We then discuss how to solve the MSPBE in (1) in both MARL and parallel RL setups with experiences.

2.2.1 Parallel RL

The parallel RL adopts multiple computing nodes to learn an optimal policy π for a specific MDP problem with high efficiency [26]. The MDP tuple of each node i is $(\mathcal{S}_i, \mathcal{A}_i, \mathcal{P}_i, \mathcal{R}_i, \gamma)$, where $\mathcal{S}_i = \mathcal{S}$, $\mathcal{A}_i = \mathcal{A}$, $\mathcal{P}_i = \mathcal{P}$ since the MDP model is identical. The local rewards may differ among nodes, but follow the same distribution and the expectation, i.e., $\mathbb{E}_{\mu^\pi}[\mathcal{R}_i(s, \mathbf{a})] = \mathbb{E}_{\mu^\pi}[\mathcal{R}_j(s, \mathbf{a})]$, $\forall (s, \mathbf{a}) \in \mathcal{S} \times \mathcal{A}, \forall i, j \in \mathcal{V}$.

Each parallel worker generates a finite sequence of trajectory $\{s_{i,p}, a_{i,p}, \mathcal{R}_i(s_{i,p}, a_{i,p})\}_{p=1}^m$ in the learning process. Based on the trajectory samples, the matrices \mathbf{A} in (1) are estimated as $\hat{\mathbf{A}} = \frac{1}{n} \sum_{i=1}^n \hat{\mathbf{A}}_i$, $\hat{\mathbf{A}}_i = \frac{1}{m} \sum_{p=1}^m \hat{\mathbf{A}}_{i,p}$, $\hat{\mathbf{A}}_{i,p} = \phi_{i,p}(\phi_{i,p} - \gamma \phi_{i,p+1})^\top$, while \mathbf{b} and \mathbf{C} are estimated analogically.

To use the distributed setting, we create each node's local copies $\{\theta_i\}$ and obtain the following form

$$\begin{aligned} \min_{\theta} \quad & \frac{1}{2} \left\| \frac{1}{N} \sum_{i=1}^n (\hat{\mathbf{A}}_i \theta_i - \hat{\mathbf{b}}_i) \right\|_{\hat{\mathbf{C}}^{-1}}^2 + \frac{1}{n} \sum_{i=1}^n \frac{\rho}{2} \|\theta_i\|^2 \\ \text{s.t.} \quad & \theta_1 = \theta_2 = \dots = \theta_N \end{aligned} \quad (2)$$

2.2.2 Collaborative MARL

In the MARL, the nodes of \mathcal{G} are heterogeneous agents which communicate and collaborate with each other [47]. Each agent observes a global state \mathbf{s} and then chooses an action $\mathbf{a}_i \in \mathcal{A}_i$ according to its local policy $\pi_i(\mathbf{a}_i|\mathbf{s})$. The joint action $\mathbf{a} = (\mathbf{a}_1, \dots, \mathbf{a}_N)$ is then executed by the group. Thus the state transition directly depends on the joint policy $\pi = (\pi_1, \dots, \pi_N)$.

Under π , the distributed agents together generate a joint trajectory $\{s_p, \mathbf{a}_p\}_{p=1}^m$, but with different reward samples $\{\mathcal{R}_i(s_p, \mathbf{a}_p)\}_{p=1}^m$ for every node $i \in \mathcal{V}$. The agents aim to collaboratively maximize the group mean reward $\mathcal{R}(s_p, \mathbf{a}_p) = \frac{1}{n} \sum_{i=1}^n \mathcal{R}_i(s_p, \mathbf{a}_p)$. The empirical MSPBE of MARL then is identical to (2), with the constraint that $\hat{\mathbf{C}}_i = \hat{\mathbf{C}}$ and $\hat{\mathbf{A}}_i = \hat{\mathbf{A}}$ for all $i \in \mathcal{V}$.

2.3 A saddle-point reformulation for the MSPBE

We design a fully asynchronous SGD method over the directed p2p network to solve the policy evaluation problem of the DisRL. To this end, we reformulate it into a summation of functions corresponding to each samples. However, (2) cannot be categorized into this type. By [9, 41], we can obtain the conjugate form of the original \mathbf{C}^{-1} -norm, i.e., $\frac{1}{2} \|\mathbf{A}\theta - \mathbf{b}\|_{\mathbf{C}^{-1}}^2 = \max_{\omega} (\omega^\top (\mathbf{A}\theta - \mathbf{b}) - \frac{1}{2} \omega^\top \mathbf{C} \omega)$, and rewrite (2) as

$$\begin{aligned} \min_{\theta} \max_{\omega} \quad & \frac{1}{MN} \sum_{i=1}^n \sum_{p=1}^m J_{i,p}(\theta_i, \omega_i) \\ \text{s.t.} \quad & \theta_1 = \theta_2 = \dots = \theta_N, \omega_1 = \omega_2 = \dots = \omega_N \end{aligned} \quad (3)$$

where $J_{i,p}(\theta_i, \omega_i) = \omega_i^\top (\hat{\mathbf{A}}_{i,p} \theta_i - \hat{\mathbf{b}}_{i,p}) - \frac{1}{2} \omega_i^\top \hat{\mathbf{C}}_{i,p} \omega_i + \frac{\rho}{2} \|\theta_i\|^2$.

Let $J_i(\theta_i, \omega_i) = \sum_{p=1}^m J_{i,p}(\theta_i, \omega_i)$ and $J(\theta, \omega) = \sum_{i=1}^n \sum_{p=1}^m J_{i,p}(\theta, \omega)$. The primal and dual stochastic gradients in (3) are given as $\nabla_{\theta_i} J_{i,p}(\theta_i, \omega_i) = \hat{\mathbf{A}}_{i,p}^\top \omega_i + \rho \theta_i$ and $\nabla_{\omega_i} J_{i,p}(\theta_i, \omega_i) = \hat{\mathbf{A}}_{i,p} \theta_i - \hat{\mathbf{C}}_{i,p} \omega_i - \hat{\mathbf{b}}_{i,p}$.

3 Algorithm and convergence analysis

3.1 The PD-APP

Motivated by the synchronous push-pull algorithm in [29], we propose the primal-dual asynchronous push-pull (PD-APP) algorithm to solve the saddle-point problem in (3) in Algorithm 1.

The PD-APP is implemented in a *fully asynchronous* way over the directed \mathcal{G} . Particularly, every node keeps receiving information from its in-neighbors and copying to its local buffers \mathcal{Z}_i^{rec} and \mathcal{S}_i^{rec} , both of which possibly contain multiple receptions from a single in-neighbor, respectively. If node i starts to update at *any* time, it simply picks a (or a batch of) random sample(s) from its local sample set and queries its buffers to perform computations in (4)-(5), where $\text{avg}(\cdot)$ and $\text{sum}(\cdot)$ return the average and sum over their arguments respectively. Then, it broadcasts the updated local variables $\tilde{\mathbf{z}}_i$ and $\tilde{\mathbf{s}}_i$ to all out-neighbors, which may also be subject to unpredictable delays, and empties both buffers. It is clear that the above process does not need any coordination with other nodes and each node is fully

Algorithm 1 The PD-APP from the view of node i

Require: Node i arbitrarily sets $\mathbf{z}_i = [\boldsymbol{\theta}_i; \boldsymbol{\omega}_i]$, initializes $\mathbf{s}_i \leftarrow \mathbf{0}, \mathbf{g}_i \leftarrow \mathbf{0}$, and creates local buffers $\mathcal{Z}_i^{rec}, \mathcal{S}_i^{rec}$.

- 1: Node i broadcasts $\tilde{\mathbf{z}}_i \leftarrow \mathbf{z}_i, \tilde{\mathbf{s}}_i \leftarrow \mathbf{s}_i / |\mathcal{N}_{out}^i|$ to all out-neighbors of i
- 2: **repeat**
- 3: Keep receiving $\tilde{\mathbf{z}}_j, \tilde{\mathbf{s}}_j$ from in-neighbors of node i and save to \mathcal{Z}_i^{rec} and \mathcal{S}_i^{rec} , respectively, until node i is ready to update.
- 4: To start a new update, node i uniformly picks a random sample indexed by $p_i \in \{1, \dots, M\}$.
- 5: Update the gradient surrogates by

$$\begin{aligned} \mathbf{z}_i &\leftarrow \text{avg}(\mathcal{Z}_i^{rec}) \\ \mathbf{g}_i^- &\leftarrow \mathbf{g}_i, \\ \mathbf{g}_i &\leftarrow [\nabla_{\boldsymbol{\theta}_i} J_{i,p_i}(\boldsymbol{\theta}_i, \boldsymbol{\omega}_i); -\nabla_{\boldsymbol{\omega}_i} J_{i,p_i}(\boldsymbol{\theta}_i, \boldsymbol{\omega}_i)] \\ \mathbf{s}_i &\leftarrow \text{sum}(\mathcal{S}_i^{rec}) + \mathbf{g}_i - \mathbf{g}_i^- . \end{aligned} \tag{4}$$

- 6: Update local primal-dual updates as

$$\tilde{\mathbf{z}}_i \leftarrow \mathbf{z}_i - \begin{bmatrix} \eta_1 \mathbf{I}_d & \mathbf{0} \\ \mathbf{0} & \eta_2 \mathbf{I}_d \end{bmatrix} \mathbf{s}_i \tag{5}$$

where $\eta_1, \eta_2 > 0$ are stepsizes.

- 7: Broadcast $\tilde{\mathbf{z}}_i \leftarrow \mathbf{z}_i$ and $\tilde{\mathbf{s}}_i \leftarrow \mathbf{s}_i / |\mathcal{N}_{out}^i|$ to all out-neighbors of node i .
 - 8: Empty \mathcal{Z}_i^{rec} and \mathcal{S}_i^{rec} .
 - 9: **until** a stopping criteria is satisfied, e.g., $\|\mathbf{s}_i\| < \epsilon$ for a predefined $\epsilon > 0$.
-

autonomous, all of which render our asynchronous model sharp contrast to the gossip-based asynchronous model [3, 23, 43] as the later involves a pair of neighbors to concurrently update with some coordination.

Unlike the distributed algorithm in [41], they require a global clock for synchronization and all nodes use the same sample per iteration, e.g., $p_i = p_j$ in Step 4 of Algorithm 1. That is, every node should access to all the samples and cannot handle decentralized sets [36], which is an important issue in the parallel RL setting.

To get a global full view of the PD-APP, we shall design a novel augmented system to convert the asynchronous update pattern into an equivalent delay-free synchronous version in Subsection 3.3, based on which the convergence of the PD-APP is established in the worst-case point of view.

3.2 Convergence result

Our analysis is based on the following assumptions.

Assumption 1. (a) (**Graph connectivity**) The digraph G is strongly connected, i.e. any pair of two nodes can be connected via a sequence of consecutive directed edges.

- (b) Let $\mathcal{T} = \{t^k\}_{k \geq 1}$ be an increasing sequence to record the updating time instants of all the nodes, e.g., $t^k \in \mathcal{T}$ if and only if one node starts a new update at time instant t^k .¹ There exists constant $b > 0$ such that for all $t^k, k \geq 1$, there is at least a new update for every node i during the time interval $[t^k, t^{k+b})$ and the broadcast variables of such a node i can be received by each of its out-neighbor node j for any $j \in \mathcal{N}_{out}^i$.

¹The probability that some nodes begin to update exactly at the same time instant is zero. If several nodes happen to update at a time instant simultaneously, we regard the nodes as updating at different time instants successively and do not violate the consistency of our result.

Assumption 2. (a) The sample amount is sufficient so that the sampled correlation matrix $\hat{\mathbf{A}}$ is full rank, and the sampled covariance $\hat{\mathbf{C}}$ is non-singular.

(b) All local stochastic gradients have bounded variances, i.e. there exist $\sigma > 0$ such that for all i, θ_i , and ω_i ,

$$\mathbb{E}\|\nabla_{\theta_i} J_{i,p_i}(\theta_i, \omega_i) - \nabla_{\theta_i} J_i(\theta_i, \omega_i)\|^2 \leq \sigma^2, \mathbb{E}\|\nabla_{\omega_i} J_{i,p_i}(\theta_i, \omega_i) - \nabla_{\omega_i} J_i(\theta_i, \omega_i)\|^2 \leq \sigma^2. \quad (6)$$

Assumption 1(a) is necessary, since otherwise there exists nodes unable to access information from some other nodes. Assumption 1(b) is easy to satisfy in practice, since the computation of each update cannot be completed instantaneously and takes a finite time. If there is an infinite time interval between two consecutive updates, it implies that such a node is dead and cannot participate in the learning process. Assumption 1(c) imposes a uniform upper bound on the unpredictable and possibly time-varying transmission delays, meaning that all the transmitted messages will be eventually successfully delivered no matter on how long it takes. It should be noted that the design and implementation of the PD-APP does not depend on such an upper bound.

Assumption 2(a) ensures the existence of a unique optimal solution for (3), while Assumption 2(b) is commonly used when analyzing the convergence rate of SGD methods, see e.g. [30]. Let θ_i^k and ω_i^k denote the latest value of the primal and dual local variables of node i just before t^k , respectively. The main theoretical result of this paper is then given below.

Theorem 1. Under Assumptions 1 and 2, we define $\{\theta^*, \omega^*\}$ as the saddle-point solution to the problem in (3) and set the step sizes as $\eta_1 = \eta, \eta_2 = \zeta\eta$. If $\zeta > \frac{4\eta + 4\lambda_{\max}(\hat{\mathbf{A}}^T \hat{\mathbf{C}}^{-1} \hat{\mathbf{A}})}{\lambda_{\min}(\hat{\mathbf{C}}^{-1})}$, the step size $\eta \in (0, \frac{\alpha\theta^4(1-\theta)^2}{24\beta^3 n^3 b^3 \tilde{t}^2})$, where the positive constants $\alpha, \beta, \theta, \tilde{t}$ are as described in Lemma 7 and Lemma 7, the expected optimality gap for each local copies in the PD-PPG, $\mathbb{E}\|\theta_i^k - \theta^*\| + \mathbb{E}\|\omega_i^k - \omega^*\|, \forall i \in \mathcal{V}, k \in \mathbb{N}$, converges to a neighborhood of the optimal solution at the rate of $\mathcal{O}(c^k), 0 < c < 1$, where the size of the neighborhood is related to n and b .

Though the linear convergence rate seems mediocre in the synchronous context, we emphasize that the virtual counter k plays an extraordinary part in our result. Unlike that synchronous works commonly use k to represent how many times the global clock clicks, in our case each update from local computing units will make a contribution to k 's increasing by 1. For the most ideal situation, n nodes with the same update frequency can increase k by $n \times 1$ while each node only performs local update once. Note that [1] have studied this kind of linear speedup elaborately.

The non-zero neighborhood in Theorem 1 is caused by the asynchronous nature of our scheme, where each node performs autonomous update without coordination. Thus, the radius of the neighborhood is related to b , the measurement of the asynchronous degree and transmission delays of the system. Since heterogenous nodes can contribute to the counter k in the same way, our theoretical result guarantees the linear performance even if in the aforementioned worst case, e.g., (a) some nodes seldom participate in the update for its poor computational ability, (b) some nodes are in bad communication status.

The detailed proof for Theorem 1 is quite lengthy. We provide a roadmap in the following two subsections. In Subsection 3.3 we advocate our augmented system and in Subsection 3.4 we provide a sketch of the proof with crucial inequality conclusions. The complete proof can be found in Appendix B.

3.3 The augmented system

Based on Assumption 1(b), we consider two individual nodes listening to incoming $\tilde{\mathbf{z}}_i, \tilde{\mathbf{s}}_i$ independently, which are denoted by $\tilde{z}_{i,0}, \tilde{s}_{i,0}$, respectively.

We further set up b virtual nodes for each $\tilde{z}_{i,0}$ node, using $\tilde{\mathcal{G}}_z = (\tilde{\mathcal{V}}_z, \tilde{\mathcal{E}}_z^k)$ to represent the (virtual) communication network of virtual nodes $\{\tilde{z}_{i,u} | 1 \leq i \leq n, 0 \leq u \leq b\}$, the overall $\tilde{n} = n(b+1)$ \mathbf{z} -nodes. In $\tilde{\mathcal{G}}_z$, the virtual nodes always send the $\tilde{\mathbf{z}}_i$ message to its following virtual nodes, i.e., $(\tilde{z}_{i,u}, \tilde{z}_{i,u+1}) \in \tilde{\mathcal{E}}_z^k$. Then, $\tilde{z}_{i,u} (u \geq 1)$ can be regarded as the future replica of the original node. If a message is sent by i at

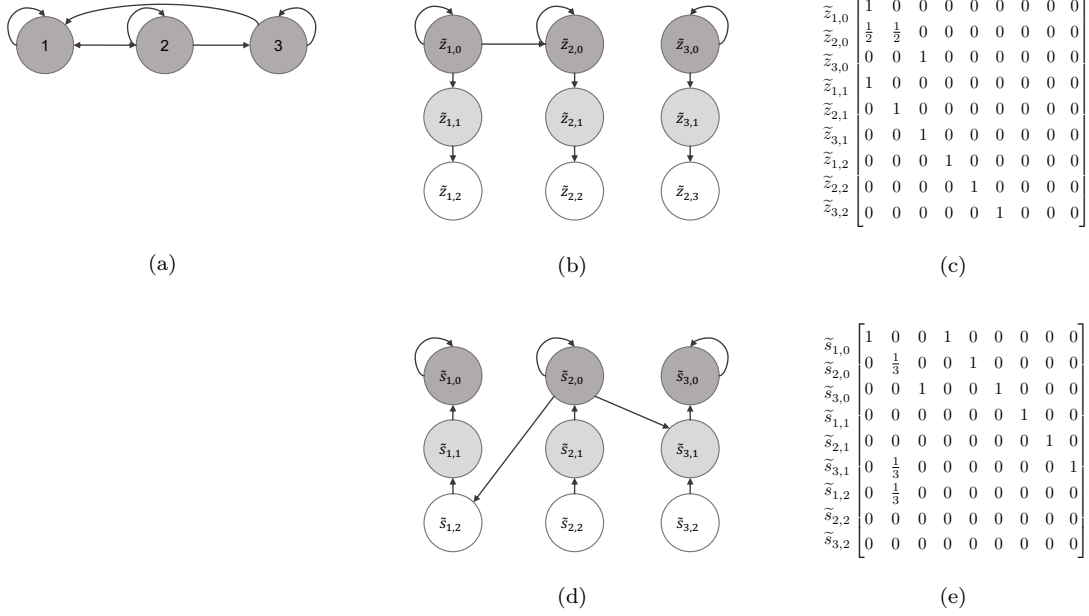


Figure 1: Consider a example with $n = 3, b = 2$, the topology of the original graph in (a). Suppose at t^k , the activated node 2 uses \mathbf{z}_2^{k-1} from itself and \mathbf{z}_1^{k-1} from node 1's latest update to compute and send out \mathbf{z}_1^k and \mathbf{s}_1^k , which are used by node 3 and 2 at t^{k+2} and t^{k+3} , respectively. (b)(d) demonstrate the virtual graphs $(\tilde{\mathcal{V}}_z, \tilde{\mathcal{E}}_z^k)$ and $(\tilde{\mathcal{V}}_s, \tilde{\mathcal{E}}_s^k)$ at time t^k . (c)(e) provide the corresponding $\tilde{\mathbf{A}}^k$ and $\tilde{\mathbf{B}}^k$. By definition, $\tilde{\mathbf{A}}^k$ and $\tilde{\mathbf{B}}^k$ are row- and column-stochastic, respectively.

the time $t^k - t^u$ and received by j at time t^k , then in the augmented system, we view its future surrogate $\tilde{z}_{i,u-1}$ as the sender and $\tilde{z}_{j,0}$ as the receiver, i.e., $(\tilde{z}_{i,u-1}, \tilde{z}_{j,0}) \in \tilde{\mathcal{E}}_z^k$.

Then we move on to \mathbf{s} 's part. Similarly, we create $\tilde{\mathcal{G}}_s = (\tilde{\mathcal{V}}_s, \tilde{\mathcal{E}}_s^k)$, where $\tilde{\mathcal{V}}_s = \{\tilde{s}_{i,u} | 1 \leq i \leq n, 0 \leq u \leq b\}$. However, the communication mode is exactly reversed, i.e., $(\tilde{s}_{i,u+1}, \tilde{s}_{i,u}) \in \tilde{\mathcal{E}}_s^k$. Meanwhile, in the \mathbf{s} -buffer, a message should wait in j 's virtual node queue and move forward before finally being used by j . If a message is sent by i at the time t^k and received by j at time $t^k + t^u$, then in the augmented system, we use $\tilde{s}_{j,u-1}$ to save the message from $\tilde{s}_{i,0}$, i.e., $(\tilde{s}_{i,0}, \tilde{s}_{j,u-1}) \in \tilde{\mathcal{E}}_s^k$. Then, it takes $u - 1$ time steps for the message in $\tilde{s}_{j,u-1}$ to reach $\tilde{s}_{j,0}$ and participate in the computation.

Suppose that node i sends message to node j at t^k , and due to delay j receives it in $(t^{k+1}, t^{k+2}]$, which is then used in update at t^{k+3} . Then, $(\tilde{z}_{i,0}, \tilde{z}_{i,1}), (\tilde{z}_{i,1}, \tilde{z}_{i,2}), (\tilde{z}_{i,2}, \tilde{z}_{j,0}) \in \tilde{\mathcal{E}}_z^{k+3}$, where $\tilde{z}_{i,2}$ is the future surrogate. Also, $(\tilde{s}_{i,0}, \tilde{s}_{j,2}), (\tilde{s}_{j,2}, \tilde{s}_{j,1}), (\tilde{s}_{j,1}, \tilde{s}_{j,0}) \in \tilde{\mathcal{E}}_s^k$, where $\tilde{z}_{j,1}, \tilde{z}_{j,2}$ play as the local queue of j . Specially, if $u = 1$ in both situations, then $(\tilde{z}_{i,0}, \tilde{z}_{j,0}) \in \tilde{\mathcal{E}}_z^{k+1}$, and $(\tilde{s}_{i,0}, \tilde{s}_{j,0}) \in \tilde{\mathcal{E}}_s^k$, respectively. The nodes are connected directly in the augmented systems as in the original one in this case.

Remark 1. By Assumption 1, $\forall k \geq 0$, \mathcal{V} is a strongly connected component in $\bigcup_{t=k}^{k+b} (\tilde{\mathcal{V}}_z, \tilde{\mathcal{E}}_z^t)$ and $\bigcup_{t=k}^{k+b} (\tilde{\mathcal{V}}_s, \tilde{\mathcal{E}}_s^t)$.

With the foundation of the augmented digraph, we now introduce the equivalent synchronous form of the original asynchronous algorithm in the following lemma.

Lemma 1. Synchronous form of PD-APP in augmented system: Let $\mathbf{z}_{i,u}^k, \mathbf{s}_{i,u}^k, 1 \leq i \leq n, 0 \leq u \leq b$ denote the value in virtual nodes $\tilde{z}_{i,u}, \tilde{s}_{i,u}$ after time t^k . For each $k \in \mathbb{N}$, there exists a row-stochastic

matrix $\tilde{\mathbf{A}}^k$ and a column-stochastic matrix $\tilde{\mathbf{B}}^k$ that can compress our asynchronous Algorithm 1 as:

$$\begin{aligned}\tilde{\mathbf{Z}}^{k+1} &= \tilde{\mathbf{A}}^k(\tilde{\mathbf{Z}}^k - \eta \mathbf{I}_a^k \tilde{\mathbf{S}}^k), \\ \tilde{\mathbf{S}}^{k+1} &= \tilde{\mathbf{B}}^k \tilde{\mathbf{S}}^k + \partial^{k+1} - \partial^k,\end{aligned}\tag{7}$$

where

$$\begin{aligned}\tilde{\mathbf{Z}}^k &= [\mathbf{Z}_0^k; \dots; \mathbf{Z}_n^k] \in \mathbb{R}^{\tilde{n} \times 2d}, \\ \mathbf{Z}_u^k &= [\mathbf{z}_{1,u}^k; \dots; \mathbf{z}_{n,u}^k] \mathbf{\Lambda}^{-1} \in \mathbb{R}^{n \times 2d}, \\ \tilde{\mathbf{S}}^k &= [\mathbf{S}_0^k; \dots; \mathbf{S}_n^k] \in \mathbb{R}^{\tilde{n} \times 2d}, \\ \mathbf{S}_u^k &= [\mathbf{s}_{1,u}^k; \dots; \mathbf{s}_{n,u}^k] \mathbf{\Lambda} \in \mathbb{R}^{n \times 2d}, \\ \partial^k &= [\partial J^k; \mathbf{0}_{bn \times 2d}] \in \mathbb{R}^{\tilde{n} \times 2d}, \\ \partial J^k &= [\partial J_1^k; \dots; \partial J_n^k] \mathbf{\Lambda} \in \mathbb{R}^{n \times 2d}, \\ \mathbf{\Lambda} &= [\mathbf{I}_d, \mathbf{0}; \mathbf{0}, \sqrt{\zeta} \mathbf{I}_d], \\ [\tilde{\mathbf{A}}^k]_{ij} &= \begin{cases} \frac{1}{|\mathcal{Z}_i^{rec,k}|}, & \text{if } j = nu + v, t^{k+1} \in \mathcal{T}_i, i \text{ receives } \mathbf{z}_j^{k-u} \text{ at } t^{k+1}, \\ 1, & \text{if } i \in \mathcal{V}, t^{k+1} \notin \mathcal{T}_i, j = i, \\ 1, & \text{if } i \notin \mathcal{V} \text{ and } j = i - n, \\ 0, & \text{otherwise,} \end{cases} \\ [\tilde{\mathbf{B}}^k]_{ji} &= \begin{cases} \frac{1}{|\mathcal{N}_{out}^i|}, & \text{if } j = nu + v, t^{k+1} \in \mathcal{T}_i, j \text{ receives } \mathbf{s}_i^k \text{ at } t^{k+u}, \\ 1, & \text{if } i \in \mathcal{V}, t^{k+1} \notin \mathcal{T}_i \text{ and } j = i, \\ 1, & \text{if } i \notin \mathcal{V} \text{ and } j = i - n, \\ 0, & \text{otherwise,} \end{cases}\end{aligned}\tag{8}$$

where $|\mathcal{Z}_i^{rec,k}|$ is the number of elements in the buffer \mathbf{Z}_i^{rec} at time t^{k+1} . Moreover,

$$[\mathbf{I}_a^k]_{ij} = \begin{cases} 1, & \text{if } i = j, i \in \mathcal{V}, \text{ and } t^{k+1} \in \mathcal{T}_i, \\ 0, & \text{otherwise.} \end{cases}$$

The stochastic gradient is sampled only when the node is activated, i.e.,

$$\begin{cases} \partial J_i^k = [\nabla_{\theta_i} J_{i,p_i^k}(\theta_i^k, \omega_i^k); \sqrt{\zeta} \nabla_{\omega_i} J_{i,p_i^k}(\theta_i^k, \omega_i^k)], & \text{if } t^k \in \mathcal{T}_i \\ \partial J_i^k = \partial J_i^{k-1}, & \text{if } t^k \notin \mathcal{T}_i \end{cases}\tag{9}$$

with $\tilde{\mathbf{Z}}^0 = [\mathbf{Z}_0^0; \mathbf{0}_{2m \times bn}]$, $\tilde{\mathbf{S}}^0 = \mathbf{0}$, and \mathcal{T}_i is an increasing sequence to record the updating time instants of node i .

We provide simple, but illuminating examples to illustrate how the augmented graphs handle delays in fig. 1 with \mathcal{G} and its corresponding $\mathcal{G}_z, \mathcal{G}_s, \tilde{\mathbf{A}}^k$, and $\tilde{\mathbf{B}}^k$ at a specific time t^k .

3.4 Proof sketch of Theorem 1

First, we introduce an important concept called *absolute probability sequence* from [38]. For any sequence of row-stochastic matrices $\{\mathbf{A}^k\}$, there exists a sequence of nonnegative stochastic vectors $\{\boldsymbol{\pi}^k\}$ that satisfies the following equations, $(\boldsymbol{\pi}^{k+1})^\top \mathbf{A}^k = (\boldsymbol{\pi}^k)^\top$, $\forall k \in \mathbb{N}$.

Then, our approach relies on the following quantities. We define

1. $\|\tilde{\mathbf{Z}}^k\|_F = \|\mathbf{T}_A^k \tilde{\mathbf{Z}}^k\|_F$, where $\mathbf{T}_A^k = \mathbf{I}_{\tilde{n}} - \mathbf{1}_{\tilde{n}}(\boldsymbol{\pi}^{k-1})^\top$, $(\boldsymbol{\pi}^{k+1})^\top \tilde{\mathbf{A}}^k = (\boldsymbol{\pi}^k)^\top$. $\|\tilde{\mathbf{Z}}^k\|_F$ is the weighted consensus error of $\tilde{\mathbf{Z}}^k$ in the augmented network.
2. $\|\tilde{\mathbf{S}}^k\|_F = \|\mathbf{T}_B^k \tilde{\mathbf{S}}^k\|_F$, where $\mathbf{T}_B^k = \mathbf{I}_{\tilde{n}} - \frac{1}{n} \mathbf{1}_{\tilde{n}}(\mathbf{v}^k)^\top$ (see also: Definition 2 in Appendix A.4.2), which is an error estimate corresponding to the gradient surrogates of distributed nodes.

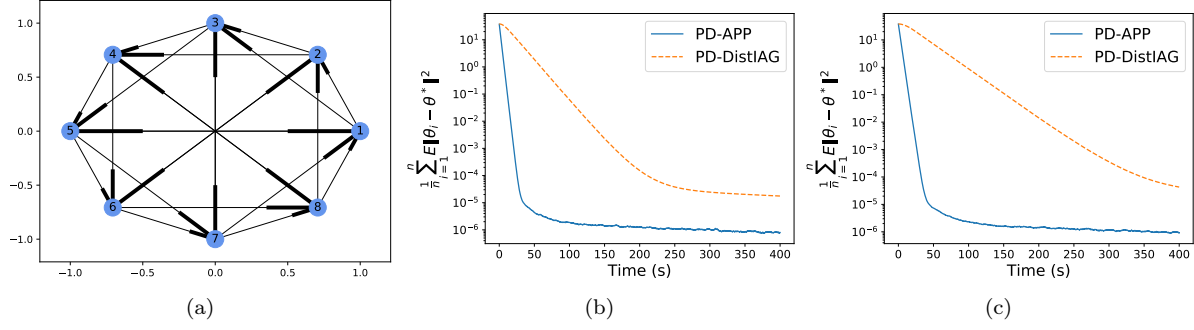


Figure 2: (a) Network topology with eight nodes. (b) Convergence performance of PD-APP and PD-distIAG with similar cores. (c) Convergence performance of PD-APP and PD-distIAG with one core slowed down.

3. $\|\tilde{\mathbf{z}}_\pi^k\|_F$, where $\tilde{\mathbf{z}}_\pi^k = \mathbf{z}_\pi^k - \mathbf{z}^* = (\tilde{\mathbf{Z}}^k)^\top \boldsymbol{\pi}^k - \mathbf{z}^*$, which is the optimality gap between the weighted average and the saddle point.

$\tilde{\mathbf{Z}}^k$, $\tilde{\mathbf{S}}_V^k$ and $\tilde{\mathbf{z}}_\pi^k$ above are bounded for all $k \geq 0$ in the four inequalities below.

$$\mathbb{E} \|\tilde{\mathbf{Z}}^{k+\tilde{t}}\|_F \leq 2\mu \mathbb{E} \|\tilde{\mathbf{Z}}^k\|_F + \eta \sqrt{2\tilde{n}} \sum_{t=0}^{\tilde{t}-1} \mathbb{E} \|\tilde{\mathbf{S}}^k\|_F, \quad (10)$$

$$\mathbb{E} \|\tilde{\mathbf{S}}_V^{k+\tilde{t}}\|_F \leq 2\beta\theta^{-1}\sqrt{\tilde{n}} \sum_{t=0}^{\tilde{t}-1} (\mathbb{E} \|\tilde{\mathbf{Z}}^{k+t}\|_F + \eta \mathbb{E} \|\tilde{\mathbf{S}}^{k+t}\|_F) + 2\theta^{-1}\mu n \mathbb{E} \|\tilde{\mathbf{S}}_V^k\|_F + 2\sqrt{2}\theta^{-1}\sqrt{\tilde{n}\tilde{t}}\zeta\sigma, \quad (11)$$

$$\mathbb{E} \|\tilde{\mathbf{z}}_\pi^{k+b}\|_F \leq (1 - \eta\alpha b n) \mathbb{E} \|\tilde{\mathbf{z}}_\pi^k\|_F + 3\eta n \beta \sum_{t=0}^{b-1} \mathbb{E} \|\tilde{\mathbf{Z}}^{k+t}\|_F + \eta n \sum_{t=0}^{b-1} \mathbb{E} \|\tilde{\mathbf{S}}_V^{k+t}\|_F + \eta n b \zeta \sigma, \quad (12)$$

$$\mathbb{E} \|\tilde{\mathbf{S}}^k\|_F \leq \beta \sqrt{\tilde{n}}(\sqrt{\tilde{n}} + 1) \mathbb{E} \|\tilde{\mathbf{Z}}^k\|_F + n \mathbb{E} \|\tilde{\mathbf{S}}_V^k\|_F + \beta n \sqrt{\tilde{n}} \mathbb{E} \|\tilde{\mathbf{z}}_\pi^k\|_F + n \sqrt{\tilde{n}} \zeta \sigma. \quad (13)$$

where μ is a constant in Corollary 1 of Appendix A.3, θ are as introduced in Lemma 6, α and β are in Lemma 7. We introduce the error vector $\mathbf{e}^k = [\mathbb{E} \|\tilde{\mathbf{Z}}^k\|_F; \mathbb{E} \|\tilde{\mathbf{S}}_V^k\|_F; \mathbb{E} \|\tilde{\mathbf{z}}_\pi^k\|_F]$, and let $\hat{\mathbf{e}}^k = [\mathbf{e}^{k+\tilde{t}-1}; \dots; \mathbf{e}^k]$. We prove that \mathbf{e}^k converges to a neighborhood of zero as $k \rightarrow \infty$ by the following lemma.

Lemma 2. *With a sufficiently small η the following inequality holds,*

$$\hat{\mathbf{e}}^{k+1} \preceq \mathbf{M}(\eta) \hat{\mathbf{e}}^k + \mathbf{w}(\sigma) \quad (14)$$

where \preceq denotes entry-wise inequality, $\tilde{t} \in \mathbb{N}^+$ can be found in Corollary 1, Appendix B.3, $\mathbf{M}(\eta) \in \mathbb{R}^{3\tilde{t} \times 3\tilde{t}}$, whose spectral radius $\rho(\mathbf{M}(\eta)) < 1$, is the upper-bounded state transition matrix and $\mathbf{w}(\sigma)$ is the error term caused by the stochasticity of the gradients and the asynchronous nature.

Note from (14), \mathbf{e}^k converges to a neighborhood of zero linearly. Clearly, since \mathbf{e}^k is bounded, then $\forall i \in \mathcal{V}$, $\mathbb{E} \|\mathbf{z}_i^k - \mathbf{z}^*\| \leq 2\mathbb{E} \|\tilde{\mathbf{Z}}^k\|_F + \mathbb{E} \|\mathbf{z}_\pi^k - \mathbf{z}^*\|$ is bounded. The result of Theorem 1 then follows.

4 Numerical results

4.1 Experiment for MARL

To compare our work with the existing works, we conducted an experiment on *mountaincar* reinforcement learning task, which was first introduced in [34]. We adopt a simple Sarsa algorithm with feature number

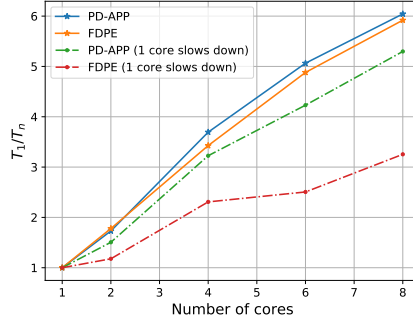


Figure 3: Speedup of PD-APP and FDPE when one core slows down. In the simulation, the computational capabilities of different CPU cores are similar. We manually slow down one core to simulate different computational speeds.

$d = 300$ to learn a fixed policy. With the given policy, we obtain trajectory experiences of states, actions and rewards of sample size $m = 5000$. To satisfy the MARL setting, we randomly divide the reward into different portions for separated nodes and make sure that we can retrieve the total reward by averaging the local rewards.

We compare our proposal to PD-distIAG [41]. In this experiment, we have eight nodes served by eight CPU cores. The network topology is the digraph counterpart of [23], i.e., each node i is able to send information to node $\text{mod}(2^j + i, n)$, where $0 \leq j < \lfloor \log_2(n) \rfloor$. The connectivity is $\mathcal{O}(\log(n))$. An eight-node example is demonstrated in Fig.2a. The learning rates for primal variables of PD-APP and PD-distIAG are 5×10^{-5} and 8×10^{-6} , which are manually selected for the best performance, and we choose $\zeta = 0.5$ for both algorithms.

In Fig. 2b, the PD-APP shows its performance in accordance with our theoretical result and confirms the converge to a neighborhood of the optimal solution at a linear rate. Then we randomly slow down one core for both algorithms. Fig.1c demonstrates that PD-APP maintains its performance while PD-distIAG suffers greatly from the slow core.

4.2 Experiment for the parallel RL

For the parallel RL, we consider the speedup effect, i.e., the more nodes the better convergence speed. On `mountaincar` task, the data $\{s_p, a_p, s_{p+1}, \mathcal{R}_i(s_p, a_p)\}_{p=1}^m$ with $d = 300, m = 24000$ are evenly divided to n -node networks. The network topology is the same as in Subsection 4.1. We compare the speedup result with FDPE [5]. We set the local batch size as $1024/n$, so that the problem has a fixed computational workload for networks with different numbers of nodes. We set $\eta = 2 \times 10^{-5}, \zeta = 0.5$ for both methods. The algorithms stop if $\|\bar{\theta}(t) - \theta^*\| \leq 10^{-3}$. We also test the robustness of both algorithms by slowing one node down. We manually add a time delay (2ms) after the node finishes each local update to simulate either poor communication situation or slow computation. Fig. 3 shows the speedup of the running time for PD-APP and FDPE, which demonstrates that PD-APP maintains its linear speedup in both situations, while FDPE, as a synchronous method, is decelerated even if only one node is disturbed.

5 Conclusion

This work has proposed a novel fully asynchronous PD-APP for policy evaluation in the disRL over a directed p2p network, which covers the MARL and parallel RL. The striking feature allows each node to communicate with its neighbors and compute its local variables at any time, without any form of coordination. In the worst-case view, we show that the PD-APP converges linearly with respect to an newly introduced virtual counter. Simulation results on the `mountaincar` have illustrated the significance of the PD-APP.

A Proof of Theorem 1

A.1 Proof of Lemma 4

We provide the explicit form of the linear inequality system in Lemma 4. The idea of the linear inequality system comes from [32]. Summarizing the results of (10)-(13), we bound $\mathbf{e}^{k+\tilde{t}}$ by

$$\begin{aligned}
\mathbf{e}^{k+\tilde{t}} \preceq & \underbrace{\begin{bmatrix} \eta\sqrt{2\tilde{n}}c_1 & \eta\sqrt{2\tilde{n}}n & \eta\sqrt{2\tilde{n}}c_2 \\ 2\beta\theta^{-1}\sqrt{\tilde{n}}(\eta c_1 + 2\sqrt{n}) & 2\beta\theta^{-1}\eta\sqrt{\tilde{n}} & 2\beta\theta^{-1}\eta c_2 \\ \eta c_3 & \eta n & 0 \end{bmatrix}}_{M_1} (\mathbf{e}^{k+\tilde{t}-1} + \dots + \mathbf{e}^{k+\tilde{t}-b+1}) \\
& + \underbrace{\begin{bmatrix} \eta\sqrt{2\tilde{n}}c_1 & \eta\sqrt{2\tilde{n}}n & \eta\sqrt{2\tilde{n}}c_2 \\ 2\beta\theta^{-1}\sqrt{\tilde{n}}(\eta c_1 + 2\sqrt{n}) & 2\beta\theta^{-1}\eta\sqrt{\tilde{n}} & 2\beta\theta^{-1}\eta c_2 \\ \eta c_3 & \eta n & 1 - \eta\alpha b n \end{bmatrix}}_{M_2} \mathbf{e}^{k+\tilde{t}-b} \\
& + \underbrace{\begin{bmatrix} \eta\sqrt{2\tilde{n}}c_1 & \eta\sqrt{2\tilde{n}}n & \eta\sqrt{2\tilde{n}}c_2 \\ 2\beta\theta^{-1}\sqrt{\tilde{n}}(\eta c_1 + 2\sqrt{n}) & 2\beta\theta^{-1}\eta\sqrt{\tilde{n}} & 2\beta\theta^{-1}\eta c_2 \\ 0 & 0 & 0 \end{bmatrix}}_{M_3} (\mathbf{e}^{k+\tilde{t}-b-1} + \dots + \mathbf{e}^{k+1}) \\
& + \underbrace{\begin{bmatrix} \eta\sqrt{2\tilde{n}}c_1 + 2\mu & \eta\sqrt{2\tilde{n}}n & \eta\sqrt{2\tilde{n}}c_2 \\ 2\beta\theta^{-1}\sqrt{\tilde{n}}[\eta c_1 + 2\sqrt{n}] & 2\beta\theta^{-1}\eta\sqrt{\tilde{n}} + 2\theta^{-1}\mu n & 2\beta\theta^{-1}\eta c_2 \\ 0 & 0 & 0 \end{bmatrix}}_{M_4} \mathbf{e}^k + \mathbf{w}(\sigma),
\end{aligned} \tag{15}$$

where $c_1 = \beta\sqrt{n\tilde{n}}(\sqrt{n} + 1)$, $c_2 = \beta n\sqrt{\tilde{n}}$ and $c_3 = 3n\beta$.

The matrix form of (15) can also be written as:

$$\hat{\mathbf{e}}^{k+\tilde{t}} \preceq \underbrace{\begin{bmatrix} \mathbf{M}_1, \dots, \mathbf{M}_1, \mathbf{M}_2, \mathbf{M}, \dots, \mathbf{M}_3, \mathbf{M}_4; \\ \mathbf{I}_{3(\tilde{t}-1)}, \mathbf{0}_{3(\tilde{t}-1) \times 3} \end{bmatrix}}_{\mathbf{M}(\eta)} \hat{\mathbf{e}}^{k+\tilde{t}-1} + \mathbf{w}(\sigma), \tag{16}$$

where

$$[\mathbf{w}(\sigma)]_i = \begin{cases} \sqrt{2}\eta n \tilde{n} \tilde{t} \underline{\zeta} \sigma, & \text{if } i = 1, \\ 2\eta\beta\theta^{-1}n\tilde{n}\tilde{t}\underline{\zeta}\sigma + 2\sqrt{2}\theta^{-1}\sqrt{\tilde{n}}\tilde{t}\underline{\zeta}\sigma, & \text{if } i = 2, \\ \eta n b \underline{\zeta} \sigma, & \text{if } i = 3, \\ 0, & \text{if } i > 3, \end{cases}$$

The matrix $\mathbf{M}(\eta)$ in (16) is exactly the one in Lemma 4 and can be further decomposed into $\mathbf{M}(\eta) = \mathbf{M}^0 + \eta\mathbf{M}^E$, i.e.,

$$\begin{aligned}
\mathbf{M}(\eta) = & \underbrace{\begin{bmatrix} \mathbf{M}_1^0, \dots, \mathbf{M}_2^0, \mathbf{M}_3^0, \dots, \mathbf{M}_3^0, \mathbf{M}_4^0; \\ \mathbf{I}_{3(\tilde{t}-1)}, \mathbf{0}_{3(\tilde{t}-1) \times 3} \end{bmatrix}}_{\mathbf{M}^0} \\
& + \eta \underbrace{\begin{bmatrix} \mathbf{M}_1^E, \dots, \mathbf{M}_2^E, \mathbf{M}_3^E, \dots, \mathbf{M}_3^E, \mathbf{M}_4^E; \\ \mathbf{0}_{3(\tilde{t}-1) \times 3\tilde{t}} \end{bmatrix}}_{\mathbf{M}^E},
\end{aligned} \tag{17}$$

where

$$\begin{aligned}
\mathbf{M}_1^0 &= \begin{bmatrix} 0 & 0 & 0 \\ 4\beta\theta^{-1}\sqrt{\tilde{n}n} & 0 & 0 \\ 0 & 0 & 0 \end{bmatrix}, & \mathbf{M}_1^E &= \begin{bmatrix} \sqrt{2\tilde{n}c_1} & \sqrt{2\tilde{n}n} & \sqrt{2\tilde{n}c_2} \\ 2\beta\theta^{-1}\sqrt{\tilde{n}c_1} & 2\beta\theta^{-1}\sqrt{\tilde{n}} & 2\beta\theta^{-1}c_2 \\ \eta c_3 & \eta n & 0 \end{bmatrix}, \\
\mathbf{M}_2^0 &= \begin{bmatrix} 0 & 0 & 0 \\ 4\beta\theta^{-1}\sqrt{\tilde{n}n} & 0 & 0 \\ 0 & 0 & 1 \end{bmatrix}, & \mathbf{M}_2^E &= \begin{bmatrix} \sqrt{2\tilde{n}c_1} & \sqrt{2\tilde{n}n} & \sqrt{2\tilde{n}c_2} \\ 2\beta\theta^{-1}\sqrt{\tilde{n}c_1} & 2\beta\theta^{-1}\sqrt{\tilde{n}} & 2\beta\theta^{-1}c_2 \\ \eta c_3 & \eta n & -\alpha bn \end{bmatrix}, \\
\mathbf{M}_3^0 &= \begin{bmatrix} 0 & 0 & 0 \\ 4\beta\theta^{-1}\sqrt{\tilde{n}n} & 0 & 0 \\ 0 & 0 & 0 \end{bmatrix}, & \mathbf{M}_3^E &= \begin{bmatrix} \sqrt{2\tilde{n}c_1} & \sqrt{2\tilde{n}n} & \sqrt{2\tilde{n}c_2} \\ 2\beta\theta^{-1}\sqrt{\tilde{n}c_1} & 2\beta\theta^{-1}\sqrt{\tilde{n}} & 2\beta\theta^{-1}c_2 \\ 0 & 0 & 0 \end{bmatrix}, \\
\mathbf{M}_4^0 &= \begin{bmatrix} 2\mu & 0 & 0 \\ 4\beta\theta^{-1}\sqrt{\tilde{n}n} & 2\theta^{-1}\mu n & 0 \\ 0 & 0 & 0 \end{bmatrix}, & \mathbf{M}_4^E &= \begin{bmatrix} \sqrt{2\tilde{n}c_1} & \sqrt{2\tilde{n}n} & \sqrt{2\tilde{n}c_2} \\ 2\beta\theta^{-1}\sqrt{\tilde{n}c_1} & 2\beta\theta^{-1}\sqrt{\tilde{n}} & 2\beta\theta^{-1}c_2 \\ 0 & 0 & 0 \end{bmatrix}.
\end{aligned}$$

To study the spectral radius of $\mathbf{M}(\eta)$, we introduce the following matrix eigenvalue perturbation lemma in [18, Theorem 6.3.12].

Lemma 3. *Let $\mathbf{A}, \mathbf{E} \in \mathbb{R}^{n \times n}$ and suppose that λ is a simple eigenvalue of \mathbf{A} . Let \mathbf{x}, \mathbf{y} be, respectively, the right and left eigenvectors of \mathbf{A} corresponding to λ . Then, there is a unique eigenvalue $\lambda(t)$ such that $\lambda(t)$ is continuous and differentiable at $t = 0$, and $\left. \frac{d\lambda(t)}{dt} \right|_{t=0} = \frac{\mathbf{y}^\top \mathbf{E} \mathbf{x}}{\mathbf{y}^\top \mathbf{x}}$.*

We next have a lemma describing the unit eigenvalue and corresponding eigenvectors of matrix \mathbf{M}_0 . [32, Appendix F] has discussed how to search the right and left eigenvectors of \mathbf{M}_0 .

Lemma 4. *The spectral radius of \mathbf{M}_0 is 1, which is also a simple eigenvalue of \mathbf{M}_0 . One pair of right and left eigenvectors \mathbf{u}, \mathbf{v} such that $\mathbf{M}_0 \mathbf{u} = \mathbf{u}$, $\mathbf{v}^\top \mathbf{M}_0 = \mathbf{v}^\top$, are given by*

$$\begin{aligned}
\mathbf{u} &= \mathbf{1}_{\tilde{t}} \otimes [0 \quad 0 \quad 1]^\top, \\
\mathbf{v}^\top &= [0, 0, 1, \underbrace{0, \dots, 0}_{(b-1) \times 3}, 0, 0, 1, \underbrace{0, \dots, 0}_{(\tilde{t}-b-1) \times 3}].
\end{aligned} \tag{18}$$

Proof. The characteristic polynomial of \mathbf{M}_0 is $(-1)^{\tilde{t}}(\lambda-1)(2\mu-\lambda^{\tilde{t}})(2\theta^{-1}\mu n-\lambda^{\tilde{t}})\lambda^{\tilde{t}-1}$, where $2\mu, 2\theta^{-1}\mu n \in (0, 1)$, given in (20) and (29), respectively. Then, it is obvious that $\varrho(\mathbf{M}_0) = 1$ and $\lambda = 1$ is a simple root of the characteristic polynomial. By direct calculation, we can verify that \mathbf{u}, \mathbf{v} are, respectively, the corresponding right and left eigenvectors of \mathbf{M}_0 . ■

Now we discuss the spectral radius of $\mathbf{M}(\eta)$ based on Lemma 3 and Lemma 4. Let $q(\eta)$ be one simple eigenvalue of $\mathbf{M}(\eta)$ satisfying that $q(0) = 1$. By Lemma 3, we obtain the derivative of $q(\eta)$, i.e., $\left. \frac{dq(\eta)}{d\eta} \right|_{\eta=0} = \frac{\mathbf{v}^\top \mathbf{M}_E \mathbf{u}}{\mathbf{v}^\top \mathbf{u}}$, where \mathbf{u}, \mathbf{v} are right and left eigenvectors of \mathbf{M}_0 corresponding to the simple eigenvalue, $q(0)$. By direct computation, it can be verified that $\mathbf{v}^\top \mathbf{u} = 2$, $\mathbf{v}^\top \mathbf{M}_E \mathbf{u} = -\alpha bn < 0$, which implies that $\left. \frac{dq(\eta)}{d\eta} \right|_{\eta=0} < 0$, i.e., the spectral radius $\varrho(\mathbf{M}(\eta)) < 1$ if η is sufficiently small, which is in accordance with the result in Lemma 4.

A.2 Discussion for the stepsize

With Lemma 3, we have proved the convergence of the system in (15) under some η . However, the explicit upper bound of η for convergence remains unknown. Noticing that in (15), the convergence is only depend on $\mathbf{M}(\eta)$, we introduce the definition of λ -sequence from [27] and a lemma in [45], and then study the convergence of $\hat{\mathbf{e}}^{k+1} \preceq \mathbf{M}(\eta) \hat{\mathbf{e}}^k$ to provide a conservative bound for η .

Definition 1. *Let $\{\mathbf{p}^t\}$ be a nonnegative sequence and $\lambda \in (0, 1)$, the λ -sequence of \mathbf{p}^k be $\mathbf{p}^{\lambda, k} = \sup_{1 \leq t \leq k} \frac{\mathbf{p}^t}{\lambda^t}$. If $\mathbf{p}^{\lambda, k}$ can be bounded by some constant \bar{p} for all k , then $\mathbf{p}^k \leq \bar{p} \lambda^k$.*

Lemma 5. [45, Lemma 5] Let $\{\mathbf{p}^k\}, \{\mathbf{q}^k\}$ be nonnegative sequences satisfying $\mathbf{p}^{t+j} \leq r\mathbf{p}^t + \sum_{i=0}^{j-1} \mathbf{q}^{t+i}$, where $r \in [0, 1)$ is a scalar. If we choose λ such that $\lambda^j \in (r, 1)$, then the λ -sequences $\mathbf{p}^{\lambda,k}$ and $\mathbf{q}^{\lambda,k}$ satisfy $\mathbf{p}^{\lambda,k} \leq \frac{j}{\lambda^j - r} \mathbf{q}^{\lambda,k} + c_\lambda$, $\forall k \in \mathbb{N}$, where $c_\lambda = \frac{\lambda^j}{\lambda^j - r} \sum_{t=1}^m \lambda^{-t} \mathbf{p}^t$ is a constant not related to k .

Based on Lemma 5 and the inequalities (10), (11), (12), and (13) without σ term, we can derive the following relationship between the λ -sequence corresponding to the above quantities. For all $k \geq 1$, if $\lambda \in \left(\max \left\{ \sqrt[\frac{i}{2}]{\frac{1}{2} + \mu}, \sqrt[\frac{i}{2}]{\frac{1}{2} + \theta^{-1}\mu n}, \sqrt[4]{1 - \eta\alpha\theta n/2} \right\}, 1\right)$, then the following inequations hold.

$$\begin{aligned} \mathbb{E}\|\tilde{\mathbf{Z}}\|_{\mathbb{F}}^{\lambda,k} &\leq \frac{2\eta n^2 \sqrt{2\tilde{n}t}}{\theta^2(n-1)} \mathbb{E}\|\tilde{\mathbf{S}}\|_{\mathbb{F}}^{\lambda,k} + p_1, \\ \mathbb{E}\|\tilde{\mathbf{S}}_{\mathbf{V}}\|_{\mathbb{F}}^{\lambda,k} &\leq \frac{4\beta\sqrt{\tilde{n}t}}{\theta^2(1-\theta)} \left(\mathbb{E}\|\tilde{\mathbf{Z}}\|_{\mathbb{F}}^{\lambda,k} + \eta \mathbb{E}\|\tilde{\mathbf{S}}\|_{\mathbb{F}}^{\lambda,k} \right) + p_2, \\ \mathbb{E}\|\tilde{\mathbf{z}}_{\pi}\|_{\mathbb{F}}^{\lambda,k} &\leq \frac{6bn\beta}{(1-\eta\alpha\theta n)\alpha\theta} \mathbb{E}\|\tilde{\mathbf{Z}}\|_{\mathbb{F}}^{\lambda,k} + \frac{2b}{(1-\eta\alpha\theta n)\alpha\theta} \mathbb{E}\|\tilde{\mathbf{S}}_{\mathbf{V}}\|_{\mathbb{F}}^{\lambda,k} + p_3 \\ \mathbb{E}\|\tilde{\mathbf{S}}\|_{\mathbb{F}}^{\lambda,k} &\leq \beta\sqrt{n\tilde{n}}(\sqrt{n}+1) \mathbb{E}\|\tilde{\mathbf{Z}}\|_{\mathbb{F}}^{\lambda,k} + n \mathbb{E}\|\tilde{\mathbf{S}}_{\mathbf{V}}(k)\|_{\mathbb{F}}^{\lambda,k} + \beta n\sqrt{\tilde{n}} \mathbb{E}\|\tilde{\mathbf{z}}_{\pi}(k)\|_{\mathbb{F}}^{\lambda,k}, \end{aligned} \quad (19)$$

where p_1, p_2, p_3 are constants not related to k , $\mathbb{E}\|\tilde{\mathbf{Z}}\|_{\mathbb{F}}^{\lambda,k}$, $\mathbb{E}\|\tilde{\mathbf{S}}_{\mathbf{V}}\|_{\mathbb{F}}^{\lambda,k}$, $\mathbb{E}\|\tilde{\mathbf{z}}_{\pi}\|_{\mathbb{F}}^{\lambda,k}$, $\mathbb{E}\|\tilde{\mathbf{S}}\|_{\mathbb{F}}^{\lambda,k}$ are the λ -sequence of $\mathbb{E}\|\tilde{\mathbf{Z}}^k\|_{\mathbb{F}}$, $\mathbb{E}\|\tilde{\mathbf{S}}_{\mathbf{V}}^k\|_{\mathbb{F}}$, $\mathbb{E}\|\tilde{\mathbf{z}}_{\pi}^k\|_{\mathbb{F}}$, $\mathbb{E}\|\tilde{\mathbf{S}}^k\|_{\mathbb{F}}$, respectively.

Let $\mathbf{d}^{\lambda,k} = [\mathbb{E}\|\tilde{\mathbf{Z}}\|_{\mathbb{F}}^{\lambda,k}; \mathbb{E}\|\tilde{\mathbf{S}}_{\mathbf{V}}\|_{\mathbb{F}}^{\lambda,k}; \mathbb{E}\|\tilde{\mathbf{z}}_{\pi}\|_{\mathbb{F}}^{\lambda,k}; \mathbb{E}\|\tilde{\mathbf{S}}\|_{\mathbb{F}}^{\lambda,k}]$, then $\mathbf{d}^{\lambda,k} \preceq \mathbf{Q}\mathbf{d}^{\lambda,k} + \mathbf{p}$, where

$$\mathbf{Q} = \begin{bmatrix} 0 & 0 & 0 & \frac{2\eta n^2 \sqrt{2\tilde{n}t}}{\theta^2(n-1)} \\ \frac{4\beta\sqrt{\tilde{n}t}}{\theta^2(1-\theta)} & 0 & 0 & \frac{4\eta\beta\sqrt{\tilde{n}t}}{\theta^2(1-\theta)} \\ \frac{6bn\beta}{(1-\eta\alpha\theta n)\alpha\theta} & \frac{2b}{(1-\eta\alpha\theta n)\alpha\theta} & 0 & 0 \\ \beta\sqrt{n\tilde{n}}(\sqrt{n}+1) & n & \beta n\sqrt{\tilde{n}} & 0 \end{bmatrix}.$$

An upper bound of η can be given by bounding $\|\mathbf{Q}^4\|_{\infty}$ to make sure that the spectral radius of \mathbf{Q} is strictly less than 1. The bound is as described in Theorem 1, i.e., $\eta \in \left(0, \frac{\alpha\theta^4(1-\theta)^2}{24\beta^3 n^3 b^3 \tilde{t}^2}\right)$.

A.3 Some preliminaries

Before proving the four claims in A.1, we first introduce some important properties of $\tilde{\mathbf{A}}^k$ and $\tilde{\mathbf{B}}^k$. We start with the accumulative products of $\tilde{\mathbf{A}}^k$ and $\tilde{\mathbf{B}}^k$, which converge to rank-one matrices linearly.

Lemma 6. ([45, Lemma 2] and [28, Lemma 5]) Define the accumulative product of $\tilde{\mathbf{A}}^k$ and $\tilde{\mathbf{B}}^k$ as

$$\Phi_{\mathbf{A}}^{k:k+t} = \tilde{\mathbf{A}}^{k+t-1} \dots \tilde{\mathbf{A}}^{k+1} \tilde{\mathbf{A}}^k, \quad \Phi_{\mathbf{B}}^{k:k+t} = \tilde{\mathbf{B}}^{k+t-1} \dots \tilde{\mathbf{B}}^{k+1} \tilde{\mathbf{B}}^k,$$

where $k \geq 0, t > 0$. If $t = 0$, define $\Phi_{\mathbf{A}}^{k:k} = \Phi_{\mathbf{B}}^{k:k} = \mathbf{I}_{\tilde{n}}$. By Assumption 1, the following statements hold.

(a) For all $k, t \geq 0$, there exist stochastic vectors $\phi_{\mathbf{A}}^{k:k+t}, \phi_{\mathbf{B}}^{k:k+t} \in \mathbb{R}^{\tilde{n}}$ such that

$$\|\Phi_{\mathbf{A}}^{k:k+t} - \mathbf{1}_{\tilde{n}}(\phi_{\mathbf{A}}^{k:k+t})^{\top}\|_{\mathbb{F}} \leq 2\kappa^t, \quad \|\Phi_{\mathbf{B}}^{k:k+t} - \phi_{\mathbf{B}}^{k:k+t} \mathbf{1}_{\tilde{n}}^{\top}\|_{\mathbb{F}} \leq 2\kappa^t,$$

where $\kappa = (1-\theta)^{1/d_g b}$ and $\theta = (1/\tilde{n})^{d_g b} \in (0, 1)$, b is as stated in Lemma 1 and d_g denotes the diameter of \mathcal{G} .

(b) For all $i \in \mathcal{V}, j \in \tilde{\mathcal{V}}_s, t \geq 0$, the following inequality is in force:

$$\sum_{j=1}^n [\Phi_{\mathbf{B}}^{0:t}]_{ij} \geq n\theta.$$

Then the following corollary follows directly, by which we introduce the constant \tilde{t} and μ to characterize the long-term convergence property of our method.

Corollary 1. *Under the conditions in Lemma 6, define $\mu < \theta/2n \in (0, 1)$. There exists a constant $\tilde{t} \geq 0$ such that $\kappa^{\tilde{t}} \leq \mu/2$, and $\forall k \geq 0$,*

$$\|\Phi_A^{k,k+\tilde{t}} - \mathbf{1}_{\tilde{n}}(\phi_A^{k,k+\tilde{t}})^\top\|_F \leq \mu, \quad \|\Phi_B^{k,k+\tilde{t}} - \phi_B^{k,k+\tilde{t}} \mathbf{1}_{\tilde{n}}^\top\|_F \leq \mu. \quad (20)$$

We use the following lemma to study the properties of \mathbf{z} and its corresponding gradients.

Lemma 7. *Let*

$$\begin{aligned} \mathbf{G}_i &= \begin{bmatrix} \eta \mathbf{I} & -\sqrt{\zeta} \hat{\mathbf{A}}_i^\top \\ \sqrt{\zeta} \hat{\mathbf{A}}_i & \zeta \hat{\mathbf{C}}_i \end{bmatrix}, \\ \nabla j_i(\mathbf{z}) &= \begin{bmatrix} \nabla_{\boldsymbol{\theta}} J_i(\boldsymbol{\theta}, \boldsymbol{\omega}) \\ -\sqrt{\zeta} \nabla_{\boldsymbol{\omega}} J_i(\boldsymbol{\theta}, \boldsymbol{\omega}) \end{bmatrix} = \begin{bmatrix} \hat{\mathbf{A}}_i^\top \boldsymbol{\omega} + \rho \boldsymbol{\theta} \\ \sqrt{\zeta} (\hat{\mathbf{A}}_i \boldsymbol{\theta} - \hat{\mathbf{C}}_i \boldsymbol{\omega} - \hat{\mathbf{b}}_i) \end{bmatrix}, \\ \mathbf{G} &= \frac{1}{n} \sum_{i=1}^n \mathbf{G}_i, \quad \nabla j(\mathbf{z}) = \frac{1}{n} \sum_{i=1}^n \nabla j_i(\mathbf{z}), \end{aligned}$$

where $\mathbf{z} = [\boldsymbol{\theta}; \boldsymbol{\omega}/\sqrt{\zeta}]$. If $\zeta = \eta_1/\eta_2$, $\eta_1 = \eta$ satisfies that $\zeta > \frac{4\eta+4\lambda_{\max}(\hat{\mathbf{A}}^\top \hat{\mathbf{C}}^{-1} \hat{\mathbf{A}})}{\lambda_{\min}(\hat{\mathbf{C}}^{-1})}$, $\eta < \lambda_{\max}(\mathbf{G})$ then there exists $\alpha = \lambda_{\min}(\mathbf{G}) > 0$, such that for all $\mathbf{z} \in \mathbb{R}^{2d}$,

$$\|\mathbf{z} - \eta \nabla j(\mathbf{z}) - \mathbf{z}^*\|_2 \leq (1 - \alpha\eta) \|\mathbf{z} - \mathbf{z}^*\|_2. \quad (21)$$

and for all $\mathbf{z}_1, \mathbf{z}_2 \in \mathbb{R}^{2d}$, $1 \leq i \leq n$,

$$\|(\nabla J_i(\mathbf{z}_1) - \nabla J_i(\mathbf{z}_2))\|_2 \leq \beta \|(\mathbf{z}_1 - \mathbf{z}_2)\|_2, \quad (22)$$

where $\beta = \max_{1 \leq i \leq n} \lambda_{\max}(\mathbf{G}_i)$.

Proof. According to [9, Appendix A], if $\zeta > \frac{4\eta+4\lambda_{\max}(\hat{\mathbf{A}}^\top \hat{\mathbf{C}}^{-1} \hat{\mathbf{A}})}{\lambda_{\min}(\hat{\mathbf{C}}^{-1})}$, the eigenvalues of \mathbf{G} are all positive. By direct computation, we can verify that

$$\mathbf{z} - \eta \nabla j(\mathbf{z}) - \mathbf{z}^* = (\mathbf{I} - \eta \mathbf{G})(\mathbf{z} - \mathbf{z}^*),$$

where $\varrho(\mathbf{I} - \eta \mathbf{G}) \leq 1 - \eta \lambda_{\min}(\mathbf{G})$. Define $\alpha = \lambda_{\min}(\mathbf{G})$ and (21) follows.

By direct computation, for all $\mathbf{z}_1, \mathbf{z}_2 \in \mathbb{R}^{2d}$, $1 \leq i \leq n$, $\nabla j_i(\mathbf{z}_1) - \nabla j_i(\mathbf{z}_2) = \mathbf{G}_i(\mathbf{z}_1 - \mathbf{z}_2)$, and (22) follows. \blacksquare

A.4 Proof of the four claims

A.4.1 Proof of (10)

Recalling Definition 1 and $\mathbf{T}_A^k = \mathbf{I}_{\tilde{n}} - \mathbf{1}_{\tilde{n}}(\boldsymbol{\pi}^{k-1})^\top$, we have

$$\begin{aligned} \|\tilde{\mathbf{Z}}^{k+\tilde{t}}\|_F &= \|\mathbf{T}_A^{k+\tilde{t}} \tilde{\mathbf{Z}}^{k+\tilde{t}}\|_F \\ &\leq \|\mathbf{T}_A^{k+\tilde{t}} \phi_A^{k:k+\tilde{t}} \tilde{\mathbf{Z}}^k\|_F + \eta \sum_{t=0}^{\tilde{t}-1} \|\mathbf{T}_A^{k+\tilde{t}} \phi_A^{k:k+\tilde{t}} \mathbf{I}_A^{k+t} \tilde{\mathbf{S}}^{k+t}\|_F. \end{aligned} \quad (23)$$

For the first term in (23), we use the property that $\boldsymbol{\pi}(k)$ is row-stochastic and get

$$\begin{aligned} \mathbf{T}_A^{k+\tilde{t}} \phi_A^{k:k+\tilde{t}} &= (\mathbf{I}_{\tilde{n}} - \mathbf{1}_{\tilde{n}}(\boldsymbol{\pi}^{k+\tilde{t}-1})^\top) \phi_A^{k:k+\tilde{t}} \\ &= (\mathbf{I}_{\tilde{n}} - \mathbf{1}_{\tilde{n}}(\boldsymbol{\pi}^{k+\tilde{t}-1})^\top) (\phi_A^{k:k+\tilde{t}} - \mathbf{1}_{\tilde{n}}(\boldsymbol{\pi}^{k-1})^\top) - (\mathbf{I}_{\tilde{n}} - \mathbf{1}_{\tilde{n}}(\boldsymbol{\pi}^{k+\tilde{t}-1})^\top) (\mathbf{1}_{\tilde{n}}(\phi_A^{k:k+\tilde{t}})^\top - \mathbf{1}_{\tilde{n}}(\boldsymbol{\pi}^{k-1})^\top) \\ &= (\mathbf{I}_{\tilde{n}} - \mathbf{1}_{\tilde{n}}(\boldsymbol{\pi}^{k+\tilde{t}-1})^\top) (\phi_A^{k:k+\tilde{t}} - \mathbf{1}_{\tilde{n}}(\phi_A^{k:k+\tilde{t}})^\top) (\mathbf{I}_{\tilde{n}} - \mathbf{1}_{\tilde{n}}(\boldsymbol{\pi}^{k-1})^\top) \\ &= \mathbf{T}_A^{k+\tilde{t}} (\phi_A^{k:k+\tilde{t}} - \mathbf{1}_{\tilde{n}}(\phi_A^{k:k+\tilde{t}})^\top) \mathbf{T}_A^k, \end{aligned} \quad (24)$$

Apply two important properties of Frobenius norm, $\|\mathbf{A}\mathbf{B}\|_F \leq \|\mathbf{A}\|_2 \|\mathbf{B}\|_F$ and $\|\mathbf{A}\mathbf{B}\|_F \leq \|\mathbf{A}\|_F \|\mathbf{B}\|_F$, and obtain

$$\begin{aligned} \|\mathbf{T}_A^{k+\tilde{t}} \phi_A^{k:k+\tilde{t}} \tilde{\mathbf{Z}}^k\|_F &\leq \|\mathbf{T}_A^{k+\tilde{t}}\|_2 \|\phi_A^{k:k+\tilde{t}} - \mathbf{1}_{\tilde{n}} \phi_A^{k:k+\tilde{t}}\|_F \|\mathbf{T}_A^k \tilde{\mathbf{Z}}^k\|_F \\ &\leq 2\mu \|\tilde{\mathbf{Z}}^k\|_F, \end{aligned} \quad (25)$$

where the last inequality is on the basis of $\|\mathbf{T}_A^{k+\tilde{t}}\|_2 = \|\mathbf{I}_{\tilde{n}} - \mathbf{1}_{\tilde{n}}(\boldsymbol{\pi}^{k+\tilde{t}-1})^\top\|_2 < 2$ and Corollary 1.

For the second term in (23),

$$\begin{aligned} \eta \sum_{t=0}^{\tilde{t}-1} \|\mathbf{T}_A^{k+\tilde{t}} \phi_A^{k:k+t} \mathbf{I}_a^{k+t} \tilde{\mathbf{S}}^{k+t}\|_F &\leq \eta \|\mathbf{T}_A^{k+\tilde{t}}\|_2 \sum_{t=0}^{\tilde{t}-1} \|\phi_A^{k:k+t} \mathbf{I}_a^{k+t} \tilde{\mathbf{S}}^{k+t}\|_F \\ &\leq \eta \sqrt{2\tilde{n}} \sum_{t=0}^{\tilde{t}-1} \|\tilde{\mathbf{S}}^{k+t}\|_F, \end{aligned} \quad (26)$$

where $\|\phi_A^{k:k+t}\|_2 \leq \sqrt{\tilde{n}/2}, \forall t \geq 0$. The desired result then follows by combining (25) and (26), and taking the full expectation on both sides.

A.4.2 Proof of (11)

Definition 2. Let $\mathbf{v}^{k+1} = \tilde{\mathbf{B}}^k \mathbf{v}^k$ and $\mathbf{v}^0 = [\mathbf{1}_n; \mathbf{0}_{\tilde{n}-n}]$. Let $\mathbf{V}^k = \text{diag}(\mathbf{v}^k)$ and $(\mathbf{V}^k)^\dagger$ be the Moore-Penrose inverse of \mathbf{V}^k , i.e.,

$$[(\mathbf{V}^k)^\dagger]_{ij} = \begin{cases} 1/[\mathbf{V}^k]_{ii}, & \text{if } i = j \leq n, [\mathbf{V}^k]_{ii} > 0, \\ 0, & \text{otherwise.} \end{cases}$$

Then, we define

$$\tilde{\mathbf{S}}_V^k = (\mathbf{V}^k)^\dagger \tilde{\mathbf{S}}^k, \quad (27)$$

where $\tilde{\mathbf{S}}^k$ is from (8).

To study $\tilde{\mathbf{S}}_V^k$, let

$$\mathbf{I}_V^k = \mathbf{V}^k (\mathbf{V}^k)^\dagger, \quad \mathbf{1}_V^k = \mathbf{I}_V^k \mathbf{1}_{\tilde{n}}, \quad \tilde{\mathbf{B}}_V^k = (\mathbf{V}^{k+1})^\dagger \tilde{\mathbf{B}}^k \mathbf{V}^k, \quad (28)$$

and define $\Phi_V^{k:k+t} = \prod_{j=k}^{k+t-1} \tilde{\mathbf{B}}_V^j$, and prove that $\Phi_V^{k:k+t}$ converges to a rank-one matrix, i.e.,

$$\left\| \Phi_V^{k:k+t} - \frac{1}{n} \mathbf{1}_V^k (\mathbf{v}^k)^\top \right\|_F < \theta^{-1} \mu n < \frac{1}{2}. \quad (29)$$

Proof. First,

$$\begin{aligned} \Phi_V^{k:k+t} &= \tilde{\mathbf{B}}_V^{k+t-1} \dots \tilde{\mathbf{B}}_V^k \\ &= (\mathbf{V}^{k+t})^\dagger \tilde{\mathbf{B}}^{k+t-1} \mathbf{I}_V^{k+t-1} \dots \tilde{\mathbf{B}}^k \mathbf{V}^k \\ &= (\mathbf{V}^{k+t})^\dagger \Phi_B^{k:k+t} \mathbf{V}^k. \end{aligned} \quad (30)$$

The last equality is tenable because $\mathbf{I}_V^{k+1} \tilde{\mathbf{B}}^k \mathbf{V}^k = \tilde{\mathbf{B}}^k \mathbf{V}^k, \forall k \geq 0$, which can be verified by computing each row on both sides, noticing $\mathbf{v}^{k+1} = \tilde{\mathbf{B}}^k \mathbf{v}^k$.

By Lemma 6(a), there exists $\Delta \Phi_B^{k:k+t} \in \mathbb{R}^{\tilde{n} \times \tilde{n}}$ such that $\|\Delta \Phi_B^{k:k+t}\|_F \leq 2\kappa^t$, and

$$\phi_B^{k:k+t} \mathbf{1}_{\tilde{n}}^\top + \Delta \Phi_B^{k:k+t} = \Phi_B^{k:k+t}.$$

Right multiply \mathbf{v}^k on both sides and yield $\phi_{\mathbf{B}}^{k:k+t} \mathbf{1}_{\tilde{n}}^{\top} \mathbf{v}^k + \Delta \Phi_{\mathbf{B}}^{k:k+t} \mathbf{v}^k = \Phi_{\mathbf{B}}^{k:k+t} \mathbf{v}^k = \mathbf{v}^{k+t}$. Since $\phi_{\mathbf{B}}^{k:k+t} \mathbf{1}_{\tilde{n}}^{\top} \mathbf{v}^k = \phi_{\mathbf{B}}^{k:k+t} \mathbf{1}_{\tilde{n}}^{\top} \mathbf{v}(0) = n \phi_{\mathbf{B}}^{k:k+t}$, we have $\phi_{\mathbf{B}}^{k:k+t} = \frac{1}{n} (\mathbf{v}^{k+t} - \Delta \Phi_{\mathbf{B}}^{k:k+t} \mathbf{v}^k)$. Then,

$$\begin{aligned} \left\| \Phi_{\mathbf{V}}^{k:k+t} - \frac{\mathbf{1}_{\tilde{n}}^k (\mathbf{v}^k)^{\top}}{n} \right\|_{\mathbf{F}} &= \left\| \Phi_{\mathbf{V}}^{k:k+t} - \frac{(\mathbf{V}^{k+t})^{\dagger} \mathbf{v}^{k+t} \mathbf{1}_{\tilde{n}}^{\top} \mathbf{V}^k}{n} \right\|_{\mathbf{F}} \\ &= \left\| (\mathbf{V}^{k+t})^{\dagger} \Delta \Phi_{\mathbf{B}}^{k:k+t} \left(\mathbf{I}_{\tilde{n}} - \frac{\mathbf{v}^k \mathbf{1}_{\tilde{n}}^{\top}}{n} \right) \right\|_{\mathbf{F}} \\ &\leq \|(\mathbf{V}^{k+t})^{\dagger}\|_2 \|\Delta \Phi_{\mathbf{B}}^{k:k+t}\|_{\mathbf{F}} \left\| \left(\mathbf{I}_{\tilde{n}} - \frac{\mathbf{v}^k \mathbf{1}_{\tilde{n}}^{\top}}{n} \right) \right\|_{\mathbf{F}} \\ &< \theta^{-1} \cdot 2\kappa^t \cdot n, \end{aligned} \quad (31)$$

where we have used the fact that all the entries of $(\mathbf{V}^k)^{\dagger}$ are less than θ^{-1} from Lemma 6(b). (29) follows directly by substituting \tilde{t} into (31). \blacksquare

Define $\mathbf{D}^k = \partial J^{k+1} - \partial J^k$ and rewrite the gradient update in (7) as $\tilde{\mathbf{S}}_{\mathbf{V}}^{k+1} = \tilde{\mathbf{B}}_{\mathbf{V}}^k \tilde{\mathbf{S}}_{\mathbf{V}}^k + (\mathbf{V}^{k+1})^{\dagger} \mathbf{D}^k$. \mathbf{D}^k is bounded for all $k \geq 0$, i.e.,

$$\mathbb{E} \|\mathbf{D}^k\|_{\mathbf{F}} \leq \beta \mathbb{E} \|\tilde{\mathbf{Z}}^k\|_{\mathbf{F}} + \beta \eta \mathbb{E} \|\tilde{\mathbf{S}}^k\|_{\mathbf{F}} + \sqrt{2} \zeta \sigma, \quad (32)$$

where β is from Lemma 7.

Proof. Define the full gradient matrix ∇^k in the same form as ∂^k , i.e.,

$$\begin{aligned} \nabla^k &= [\nabla J(k); \mathbf{0}_{bn \times 2d}] \in \mathbb{R}^{\tilde{n} \times 2d}, \\ \nabla J^k &= [\nabla J_1(k); \dots; \nabla J_n(k)] \in \mathbb{R}^{n \times 2d}, \\ \nabla J_i^k &= [\nabla_{\theta_i} J_i(\theta_i(k), \omega_i(k)); -\sqrt{\zeta} \nabla_{\omega_i} J_i(\theta_i(k), \omega_i(k))], \quad 1 \leq i \leq n, \end{aligned} \quad (33)$$

and let $\nabla J^0 = \mathbf{0}$.

Using triangle inequality, we obtain that

$$\begin{aligned} \mathbb{E} \|\mathbf{D}^k\|_{\mathbf{F}} &= \mathbb{E} \|(\partial J^{k+1} - \partial J^k)\|_{\mathbf{F}} \\ &\leq \mathbb{E} \|\mathbf{I}_a^k (\partial J^{k+1} - \partial J^k - \nabla J^{k+1} + \nabla J^k)\|_{\mathbf{F}} + \mathbb{E} \|\mathbf{I}_a^k (\nabla J^{k+1} - \nabla J^k)\|_{\mathbf{F}} \\ &\leq \beta \mathbb{E} \|\mathbf{I}_a^k (\tilde{\mathbf{Z}}^{k+1} - \tilde{\mathbf{Z}}^k)\|_{\mathbf{F}} + \sqrt{2} \zeta \sigma \\ &\leq \beta \mathbb{E} \|(\mathbf{I}_a^k \tilde{\mathbf{A}}^k - \mathbf{I}_a^k) \mathbf{T}_A^k \tilde{\mathbf{Z}}^k\|_{\mathbf{F}} + \beta \eta \mathbb{E} \|\tilde{\mathbf{S}}^k\|_{\mathbf{F}} + \sqrt{2} \zeta \sigma \\ &\leq \beta \mathbb{E} \|\tilde{\mathbf{Z}}^k\|_{\mathbf{F}} + \eta \beta \mathbb{E} \|\tilde{\mathbf{S}}^k\|_{\mathbf{F}} + \sqrt{2} \zeta \sigma, \end{aligned} \quad (34)$$

where $\zeta = \sqrt{1 + \zeta}$. The third inequality follows from (22), (6) and the independency between $\mathbf{I}_a^k \partial J^{k+1}$ and $\mathbf{I}_a^k \partial J^k$. The last inequalities is based on the row-stochasticity of $\tilde{\mathbf{A}}^k$. \blacksquare

With the preparations above, we prove (11) in a similar way as in the previous subsection, Appendix A.4.1. From the update in (7), we get

$$\begin{aligned} \|\tilde{\mathbf{S}}_{\mathbf{V}}^{k+\tilde{t}}\|_{\mathbf{F}} &= \left\| \mathbf{T}_{\mathbf{B}}^{k+\tilde{t}} \tilde{\mathbf{S}}_{\mathbf{V}}^{k+\tilde{t}} \right\|_{\mathbf{F}} \\ &\leq \left\| \mathbf{T}_{\mathbf{B}}^{k+\tilde{t}} \Phi_{\mathbf{V}}^{k:k+\tilde{t}} \tilde{\mathbf{S}}_{\mathbf{V}}^k \right\|_{\mathbf{F}} + \sum_{t=0}^{\tilde{t}-1} \left\| \left(\mathbf{I}_{\mathbf{V}}^{k+\tilde{t}} - \frac{1}{n} \mathbf{1}_{\mathbf{V}}^{k+\tilde{t}} (\mathbf{v}^{k+\tilde{t}})^{\top} \right) \Phi_{\mathbf{V}}^{k+t+1:k+\tilde{t}} (\mathbf{V}^{k+t+1})^{\dagger} \mathbf{D}^{k+t} \right\|_{\mathbf{F}} \\ &\leq 2\theta^{-1} \mu n \|\tilde{\mathbf{S}}_{\mathbf{V}}^k\|_{\mathbf{F}} + \sum_{t=0}^{\tilde{t}-1} 2\sqrt{\tilde{n}} \theta^{-1} \|\mathbf{D}^{k+t}\|_{\mathbf{F}}, \end{aligned} \quad (35)$$

where the last inequality is from (29). The first term of the second row in (35) can be verified in the same way as in (24). (35) along with (32) implies the desired result (11).

A.4.3 Proof of (12)

By definition, $(\tilde{\mathbf{z}}_\pi^k)^\top = (\boldsymbol{\pi}^k)^\top \tilde{\mathbf{Z}}^k - (\mathbf{z}^*)^\top$. Repeating the first step in the above two proofs, we get

$$\begin{aligned} (\mathbf{z}_\pi^{k+b})^\top &= (\boldsymbol{\pi}^{k+b})^\top \tilde{\mathbf{Z}}^{k+b} \\ &= (\boldsymbol{\pi}^{k+b})^\top \boldsymbol{\Phi}_A^{k:k+b} \tilde{\mathbf{Z}}^{k+b} - \eta (\boldsymbol{\pi}^{k+b})^\top \sum_{t=0}^{b-1} \boldsymbol{\Phi}_A^{k+t+1:k+b} \mathbf{I}_a^{k+t} \mathbf{V}^{k+t} \check{\mathbf{S}}_V^{k+t} \\ &= (\mathbf{z}_\pi^k)^\top - \eta (\boldsymbol{\pi}^{k+b})^\top \sum_{t=0}^{b-1} \boldsymbol{\Phi}_A^{k+t+1:k+b} \mathbf{I}_a^{k+t} \mathbf{V}^{k+t} \check{\mathbf{S}}_V^{k+t}. \end{aligned} \quad (36)$$

We try to extract the global gradient ingredient in (36) (the gradient of $J(\boldsymbol{\theta}, \boldsymbol{\omega})$ instead of $J_i(\boldsymbol{\theta}, \boldsymbol{\omega})$) by defining

$$\begin{aligned} (\mathbf{r}^{k,t})^\top &= \eta (\boldsymbol{\pi}^{k+b})^\top \boldsymbol{\Phi}_A^{k+t+1:k+b} \mathbf{I}_a^{k+t} \mathbf{V}^{k+t}, \\ \eta^{k,t} &= (\mathbf{r}^{k,t})^\top \mathbf{1}_V^{k+t}, \quad \underline{\eta}^k = \sum_{t=0}^{b-1} \eta^{k,t}, \end{aligned}$$

where \mathbf{V}^k and $\mathbf{1}_V^k$ are defined in Definition 2 and (28), respectively. By introducing $\nabla j(\mathbf{z}_\pi^k)$, the global gradient of \mathbf{z}_π^k , the last row in (36) is decomposed into

$$\begin{aligned} (\mathbf{z}_\pi^{k+b} - \mathbf{z}^*)^\top &= (\mathbf{z}_\pi^k - \mathbf{z}^* - \underline{\eta}^k \nabla j(\mathbf{z}_\pi^k))^\top \\ &\quad + \sum_{t=0}^{b-1} \eta^{k,t} \left(\nabla j(\mathbf{z}_\pi^k)^\top - \frac{1}{n} \mathbf{1}_{\tilde{n}}^\top \nabla^{k+t} \right) \\ &\quad - \sum_{t=0}^{b-1} (\mathbf{r}^{k,t})^\top \left(\check{\mathbf{S}}_V^{k+t} - \frac{1}{n} (\mathbf{1}_V^{k+t})^\top \mathbf{1}_{\tilde{n}}^\top \nabla^{k+t} \right) \\ &\quad + \sum_{t=0}^{b-1} \eta^{k,t} \left[\frac{1}{n} \mathbf{1}_{\tilde{n}}^\top (\nabla^{k+t} - \partial^{k+t}) \right]. \end{aligned} \quad (37)$$

The first row of (37), $\mathbf{z}_\pi^k - \mathbf{z}^* - \underline{\eta}^k \nabla j(\mathbf{z}_\pi^k)$, depicts the full gradient ascent/descent of the weight average variables \mathbf{z}_π^k , while the second to the fourth rows are error terms that are bounded, as in (38)-(40).

First, notice that for all $k \geq 0, t \geq 0$, we have $\eta^{k,t} \leq \eta n$ and $\underline{\eta}^k \leq \eta b n$. Applying Lemma 7, we have $\|\mathbf{z}_\pi^k - \mathbf{z}^* - \underline{\eta}^k \nabla j(\mathbf{z}_\pi^k)\|_F \leq (1 - \eta \alpha b n) \|\mathbf{z}_\pi^k - \mathbf{z}^*\|_F$.

Second, let $\mathbf{1}_{n|\tilde{n}} = [\mathbf{1}_n; \mathbf{0}_{\tilde{n}-n}] \in \mathbb{R}^{\tilde{n}}$, and $\mathbf{I}_{n|\tilde{n}} \in \mathbb{R}^{\tilde{n} \times \tilde{n}}: [\mathbf{I}_{n|\tilde{n}}]_{ij} = \begin{cases} 1, & \text{if } i = j \leq n, \\ 0, & \text{otherwise.} \end{cases}$

By direct computation, $\nabla j(\mathbf{z})^\top = n^{-1} \mathbf{1}_n^\top \nabla J(\mathbf{1}_n \mathbf{z}^\top)$, $\forall \mathbf{z}$. From (33), we obtain that for all k , $\mathbf{1}_{\tilde{n}}^\top \nabla^k = \mathbf{1}_{n|\tilde{n}}^\top \nabla^k = \mathbf{1}_n^\top \nabla J(\mathbf{Z}_0^k)$. Then,

$$\begin{aligned} &\left\| \sum_{t=0}^{b-1} \eta^{k,t} \left(\nabla j(\mathbf{z}_\pi^k)^\top - \frac{1}{n} \mathbf{1}_{\tilde{n}}^\top \nabla^{k+t} \right) \right\|_F \\ &= \left\| \sum_{t=0}^{b-1} \frac{\eta^{k,t}}{n} (\mathbf{1}_n^\top \nabla J(\mathbf{1}_n (\mathbf{z}_\pi^k)^\top) - \mathbf{1}_n^\top \nabla J(\mathbf{Z}_0^{k+t})) \right\|_F \\ &\leq \eta \sqrt{n} \beta \sum_{t=0}^{b-1} \left\| (\mathbf{1}_{n|\tilde{n}}^\top (\mathbf{z}_\pi^k)^\top - \mathbf{1}_{n|\tilde{n}}^\top \boldsymbol{\pi}^{k+t-1} \tilde{\mathbf{Z}}^{k+t}) \right\|_F \\ &\leq 3\eta m \beta \sum_{t=0}^{b-1} \|\tilde{\mathbf{Z}}^{k+t}\|_F, \end{aligned} \quad (38)$$

where the first inequality follows from (22).

Third, by (7) and (28), then,

$$\begin{aligned}
& \left\| \sum_{t=0}^{b-1} (\mathbf{r}^{k,t})^\top \left(\mathbf{S}_V^{k+t} - \frac{1}{n} \mathbf{1}_V^{k+t} \mathbf{1}_{\tilde{n}}^\top \partial^{k+t} \right) \right\|_F \\
&= \left\| \sum_{t=0}^{b-1} (\mathbf{r}^{k,t})^\top \left(\mathbf{S}_V^{k+t} - \frac{1}{n} \mathbf{1}_V^{k+t} (\mathbf{v}^{k+t})^\top \mathbf{S}_V^{k+t} \right) \right\|_F \\
&\leq \sum_{t=0}^{b-1} \|\mathbf{r}^{k,t}\|_2 \|\tilde{\mathbf{S}}^{k+t}\|_F \leq \eta n \sum_{t=0}^{b-1} \|\tilde{\mathbf{S}}^{k+t}\|_F.
\end{aligned} \tag{39}$$

Moreover, it follows from (6) that

$$\mathbb{E} \left\| \sum_{t=0}^{b-1} \eta^{k,t} \left[\frac{1}{n} \mathbf{1}_{\tilde{n}}^\top (\nabla^{k+t} - \partial^{k+t}) \right] \right\|_F \leq \eta n b \underline{\zeta} \sigma. \tag{40}$$

Finally, one can summarize (37)-(40) and take expectation to get the final result of (12).

A.4.4 Proof of (13)

By (27), it holds that $\mathbf{1}_{\tilde{n}}^\top \partial^k = (\mathbf{v}^{k+t})^\top \mathbf{S}_V^k$ and

$$\begin{aligned}
\|\tilde{\mathbf{S}}^k\|_F &= \|\mathbf{V}^k \mathbf{T}_B^k \mathbf{S}_V^k + \frac{1}{n} V^k (\mathbf{1}_V^k)^\top (\mathbf{v}^{k+t})^\top \mathbf{S}_V^k\|_F \\
&\leq \|\mathbf{V}^k\|_2 \|\mathbf{T}_B^k \mathbf{S}_V^k\|_F + \left\| \frac{1}{n} V^k \mathbf{1}_V^k \mathbf{1}_{\tilde{n}}^\top \partial^k \right\|_F \\
&\leq n \|\tilde{\mathbf{S}}_V^k\|_F + \|\mathbf{1}_V^k \mathbf{1}_{\tilde{n}}^\top \partial^k\|_F.
\end{aligned} \tag{41}$$

For the expectation of second term in (41), we have

$$\begin{aligned}
\mathbb{E} \|\mathbf{1}_V^k \mathbf{1}_{\tilde{n}}^\top \partial^k\|_F &= \mathbb{E} \left\| \mathbf{1}_V^k \left(\mathbf{1}_{\tilde{n}}^\top \partial J^k - \mathbf{1}_{\tilde{n}}^\top \nabla J(\mathbf{1}_n(\mathbf{z}^*)^\top) \right) \right\|_F \\
&\leq \mathbb{E} \left\| \mathbf{1}_V^k \mathbf{1}_{\tilde{n}}^\top \right\|_2 \left(\|\nabla J^k - \nabla J(\mathbf{1}_n(\mathbf{z}^*)^\top)\|_F + \|(\partial J^k - \nabla J^k)\|_F \right) \\
&\leq \mathbb{E} \sqrt{n\tilde{n}} \|\nabla J^k - \nabla J(\mathbf{1}_n(\mathbf{z}^*)^\top)\|_F + \sqrt{n\tilde{n}} \underline{\zeta} \sigma \\
&\leq \beta \sqrt{n\tilde{n}} \mathbb{E} \|(\mathbf{I}_{n|\tilde{n}} \tilde{\mathbf{Z}}^k - \mathbf{1}_{n|\tilde{n}}(\mathbf{z}^*)^\top)\|_F + \sqrt{n\tilde{n}} \underline{\zeta} \sigma \\
&\leq \beta \sqrt{n\tilde{n}} \mathbb{E} \left\| \left(\mathbf{I}_{n|\tilde{n}} \tilde{\mathbf{Z}}^k - \mathbf{1}_{n|\tilde{n}}(\boldsymbol{\pi}^{k-1})^\top \right) \tilde{\mathbf{Z}}^k \right\|_F + \beta \sqrt{n\tilde{n}} \mathbb{E} \left\| \mathbf{1}_{n|\tilde{n}} \left((\boldsymbol{\pi}^{k-1})^\top \tilde{\mathbf{Z}}^k - (\mathbf{z}^*)^\top \right) \right\|_F + \sqrt{n\tilde{n}} \underline{\zeta} \sigma \\
&\leq \beta \sqrt{n\tilde{n}} (\sqrt{n} + 1) \mathbb{E} \|\tilde{\mathbf{Z}}^k\|_F + \beta \sqrt{\tilde{n}} n \mathbb{E} \|(\mathbf{z}_\pi^k - \mathbf{z}^*)^\top\|_F + \sqrt{n\tilde{n}} \underline{\zeta} \sigma
\end{aligned} \tag{42}$$

Thus, we obtain (13) by using (41) and (42).

References

- [1] Mahmoud Assran and Michael Rabbat. An empirical comparison of multi-agent optimization algorithms. In *IEEE Global Conference on Signal and Information Processing*, pages 573–577. IEEE, 2017.
- [2] Mahmoud Assran and Michael Rabbat. Asynchronous subgradient-push. *arXiv preprint arXiv:1803.08950*, 2018.

- [3] Mahmoud ("Mido") Assran, Joshua Romoff, Nicolas Ballas, Joelle Pineau, and Mike Rabbat. Gossip-based actor-learner architectures for deep reinforcement learning. In *Advances in Neural Information Processing Systems*, pages 13299–13309, 2019.
- [4] Dimitri P Bertsekas and John N Tsitsiklis. *Parallel and distributed computation: numerical methods*. Athena Scientific, 1989.
- [5] Lucas Cassano, Kun Yuan, and Ali H Sayed. Distributed value-function learning with linear convergence rates. In *18th European Control Conference*, pages 505–511. IEEE, 2019.
- [6] Tianyi Chen, Kaiqing Zhang, Georgios B Giannakis, and Tamer Başar. Communication-efficient distributed reinforcement learning. *arXiv preprint arXiv:1812.03239*, 2018.
- [7] Dongsheng Ding, Xiaohan Wei, Zhuoran Yang, Zhaoran Wang, and Mihailo R Jovanović. Fast multi-agent temporal-difference learning via homotopy stochastic primal-dual optimization. *arXiv preprint arXiv:1908.02805*, 2019.
- [8] Thinh Doan, Siva Maguluri, and Justin Romberg. Finite-time analysis of distributed TD(0) with linear function approximation on multi-agent reinforcement learning. In *International Conference on Machine Learning*, pages 1626–1635, 2019.
- [9] Simon S Du, Jianshu Chen, Lihong Li, Lin Xiao, and Dengyong Zhou. Stochastic variance reduction methods for policy evaluation. In *International Conference on Machine Learning*, pages 1049–1058, 2017.
- [10] Lasse Espeholt, Hubert Soyer, Remi Munos, Karen Simonyan, Vlad Mnih, Tom Ward, Yotam Doron, Vlad Firoiu, Tim Harley, Iain Dunning, Shane Legg, and Koray Kavukcuoglu. IMPALA: Scalable distributed deep-RL with importance weighted actor-learner architectures. In *International Conference on Machine Learning*, pages 1407–1416, 2018.
- [11] Weiming Feng, Thomas Hayes, and Yitong Yin. Distributed metropolis sampler with optimal parallelism. *arXiv preprint arXiv: 1904.00943*, 2019.
- [12] Jakob Foerster, Ioannis Alexandros Assael, Nando de Freitas, and Shimon Whiteson. Learning to communicate with deep multi-agent reinforcement learning. In *Advances in Neural Information Processing Systems*, pages 2137–2145, 2016.
- [13] Scott Fujimoto, Herke Hoof, and David Meger. Addressing function approximation error in actor-critic methods. In *International Conference on Machine Learning*, pages 1587–1596, 2018.
- [14] Ivo Grondman, Lucian Busoniu, Gabriel AD Lopes, and Robert Babuska. A survey of actor-critic reinforcement learning: Standard and natural policy gradients. *IEEE Transactions on Systems, Man, and Cybernetics, Part C (Applications and Reviews)*, 42(6):1291–1307, 2012.
- [15] Jayesh K Gupta, Maxim Egorov, and Mykel Kochenderfer. Cooperative multi-agent control using deep reinforcement learning. In *International Conference on Autonomous Agents and Multiagent Systems*, pages 66–83, 2017.
- [16] Tuomas Haarnoja, Aurick Zhou, Pieter Abbeel, and Sergey Levine. Soft actor-critic: Off-policy maximum entropy deep reinforcement learning with a stochastic actor. In *International Conference on Machine Learning*, pages 1861–1870, 2018.
- [17] Robert Hannah, Fei Feng, and Wotao Yin. A2BCD: asynchronous acceleration with optimal complexity. In *International Conference on Learning Representations*, 2019.
- [18] Roger A Horn and Charles R Johnson. *Matrix analysis*. Cambridge university press, 2012.

- [19] Steven Kapturowski, Georg Ostrovski, John Quan, Remi Munos, and Will Dabney. Recurrent experience replay in distributed reinforcement learning. In *International Conference on Learning Representations*, 2019.
- [20] Soumya Kar, José MF Moura, and H Vincent Poor. Qd-learning: A collaborative distributed strategy for multi-agent reinforcement learning through consensus+innovations. *IEEE Transactions on Signal Processing*, 61:1848–1862, 2013.
- [21] Jens Kober, J Andrew Bagnell, and Jan Peters. Reinforcement learning in robotics: A survey. *The International Journal of Robotics Research*, 32(11):1238–1274, 2013.
- [22] Xiangru Lian, Ce Zhang, Huan Zhang, Cho-Jui Hsieh, Wei Zhang, and Ji Liu. Can decentralized algorithms outperform centralized algorithms? a case study for decentralized parallel stochastic gradient descent. In *Advances in Neural Information Processing Systems*, pages 5330–5340, 2017.
- [23] Xiangru Lian, Wei Zhang, Ce Zhang, and Ji Liu. Asynchronous decentralized parallel stochastic gradient descent. In *International Conference on Machine Learning*, pages 3043–3052, 2018.
- [24] Ji Liu and Stephen J Wright. Asynchronous stochastic coordinate descent: Parallelism and convergence properties. *SIAM Journal on Optimization*, 25(1):351–376, 2015.
- [25] Patrick Mannion, Karl Mason, Sam Devlin, Jim Duggan, and Enda Howley. Dynamic economic emissions dispatch optimisation using multi-agent reinforcement learning. In *Proceedings of the Adaptive and Learning Agents Workshop (at AAMAS 2016)*, 2016.
- [26] Volodymyr Mnih, Adria Puigdomenech Badia, Mehdi Mirza, Alex Graves, Timothy Lillicrap, Tim Harley, David Silver, and Koray Kavukcuoglu. Asynchronous methods for deep reinforcement learning. In *International Conference on Machine Learning*, pages 1928–1937, 2016.
- [27] Angelia Nedic, Alex Olshevsky, and Wei Shi. Achieving geometric convergence for distributed optimization over time-varying graphs. *SIAM Journal on Optimization*, 27(4):2597–2633, 2017.
- [28] Angelia Nedić and Asuman Ozdaglar. Convergence rate for consensus with delays. *Journal of Global Optimization*, 47(3):437–456, 2010.
- [29] Shi Pu, Wei Shi, Jinming Xu, and Angelia Nedić. A push-pull gradient method for distributed optimization in networks. *arXiv preprint arXiv:1803.07588*, 2018.
- [30] Chao Qu, Shie Mannor, Huan Xu, Yuan Qi, Le Song, and Junwu Xiong. Value propagation for decentralized networked deep multi-agent reinforcement learning. In *Advances in Neural Information Processing Systems*, pages 1182–1191, 2019.
- [31] Jineng Ren and Jarvis Haupt. A communication efficient hierarchical distributed optimization algorithm for multi-agent reinforcement learning. In *Real-world Sequential Decision Making Workshop at International Conference on Machine Learning*, 2019.
- [32] Fakhteh Saadatniaki, Ran Xin, and Usman A Khan. Decentralized optimization over time-varying directed graphs with row and column-stochastic matrices. *IEEE Transactions on Automatic Control*, 2020.
- [33] Kevin Scaman, Francis Bach, Sebastien Bubeck, Laurent Massoulié, and Yin Tat Lee. Optimal algorithms for non-smooth distributed optimization in networks. In *Advances in Neural Information Processing Systems*, pages 2740–2749, 2018.
- [34] Richard S Sutton and Andrew G Barto. *Reinforcement learning: An introduction*. MIT press, 2018.

- [35] Richard S Sutton, Hamid Reza Maei, Doina Precup, Shalabh Bhatnagar, David Silver, Csaba Szepesvári, and Eric Wiewiora. Fast gradient-descent methods for temporal-difference learning with linear function approximation. In *Annual International Conference on Machine Learning*, pages 993–1000. ACM, 2009.
- [36] Hanlin Tang, Xiangru Lian, Ming Yan, Ce Zhang, and Ji Liu. d^2 : Decentralized training over decentralized data. In *International Conference on Machine Learning*, pages 4848–4856, 2018.
- [37] Ye Tian, Ying Sun, and Gesualdo Scutari. Achieving linear convergence in distributed asynchronous multi-agent optimization. *arXiv preprint arXiv:1803.10359*, 2018.
- [38] Behrouz Touri. *Product of random stochastic matrices and distributed averaging*. Springer Science & Business Media, 2012.
- [39] Elise Van der Pol and Frans A Oliehoek. Coordinated deep reinforcement learners for traffic light control. *Proceedings of Learning, Inference and Control of Multi-Agent Systems (at NIPS 2016)*, 2016.
- [40] Oriol Vinyals, Igor Babuschkin, Wojciech M Czarnecki, Michaël Mathieu, Andrew Dudzik, Junyoung Chung, David H Choi, Richard Powell, Timo Ewalds, Petko Georgiev, et al. Grandmaster level in starcraft ii using multi-agent reinforcement learning. *Nature*, 575(7782):350–354, 2019.
- [41] Hoi-To Wai, Zhuoran Yang, Princeton Zhaoran Wang, and Mingyi Hong. Multi-agent reinforcement learning via double averaging primal-dual optimization. In *Advances in Neural Information Processing Systems*, pages 9649–9660, 2018.
- [42] Kan Xie, Qianqian Cai, and Minyue Fu. A fast clock synchronization algorithm for wireless sensor networks. *Automatica*, 92:133–142, 2018.
- [43] Jinming Xu, Shanying Zhu, Yeng Chai Soh, and Lihua Xie. Convergence of asynchronous distributed gradient methods over stochastic networks. *IEEE Transactions on Automatic Control*, 63(2):434–448, 2017.
- [44] Jiaqi Zhang and Keyou You. Asynchronous decentralized optimization in directed networks. *arXiv preprint arXiv:1901.08215*, 2019.
- [45] Jiaqi Zhang and Keyou You. Asynchronous decentralized optimization in directed networks. *arXiv preprint arXiv:1901.08215*, 2019.
- [46] Jiaqi Zhang and Keyou You. Asyspa: An exact asynchronous algorithm for convex optimization over digraphs. *IEEE Transactions on Automatic Control*, 2019.
- [47] Kaiqing Zhang, Zhuoran Yang, and Tamer Başar. Multi-agent reinforcement learning: A selective overview of theories and algorithms. *arXiv preprint arXiv:1911.10635*, 2019.
- [48] Kaiqing Zhang, Zhuoran Yang, Han Liu, Tong Zhang, and Tamer Basar. Fully decentralized multi-agent reinforcement learning with networked agents. In *International Conference on Machine Learning*, pages 5872–5881, 2018.
- [49] Yan Zhang and Michael M Zavlanos. Distributed off-policy actor-critic reinforcement learning with policy consensus. *arXiv preprint arXiv:1903.09255*, 2019.